R. & M. No. 2920
(15,260)
A.R.C. Technical Report

MINISTRY OF SUPPLY

AERONAUTICAL RESEARCH COUNCIL
REPORTS AND MEMORANDA

Analysis of Reynolds Number Effects in Fluid Flow through Two-dimensional Cascades

By

D. J. K. STUART, M.A., Ph.D.,
of University Engineering Department, Cambridge

LONDON : HER MAJESTY'S STATIONERY OFFICE
1955
PRICE 10s 6d NET

Analysis of Reynolds Number Effects in Fluid Flow through Two-dimensional Cascades

By

D. J. K. STUART, M.A., Ph.D.,
of the University Engineering Department, Cambridge

COMMUNICATED BY THE PRINCIPAL DIRECTOR OF SCIENTIFIC RESEARCH (AIR),
MINISTRY OF SUPPLY

Reports and Memoranda No. 2920

July, 1952

Summary.—This report describes an investigation into the effects of Reynolds number on the flow through two dimensional cascades of the diffusing type. Particular emphasis has been placed on the causes of high loss especially at very low Reynolds numbers. Separation of both the laminar and turbulent boundary layers are verified as sources of low efficiency in this particular type of flow and these phenomena have, consequently, been studied in considerable detail.

The main work consists of approximate mathematical analysis of representative flows but this theoretical work has been carried out in conjunction with, and is supported by, results drawn from an extensive programme of tests made in the low-speed wind tunnel at the Cambridge University Engineering Laboratory. These tests are fully described in Ref. 1. Mach number effects were specifically avoided in the experimental work although a wide range of Reynolds number ($3{\cdot}0 \times 10^4$ to $5{\cdot}0 \times 10^5$) was covered; the effects of compressibility have not, therefore, been considered in the main analysis.

The transition to turbulent flow in the boundary layer is shown to be of vital importance in determining the pattern of flow, especially at low Reynolds numbers where laminar breakaway is likely to occur, and the need for a theoretical or semi-empirical method of predicting transition is stressed.

In the theoretical work the generally accepted approach has been followed in that the potential flow pattern has been used as a basis for further calculation. The close agreement of the analysis with the experimental results has justified the use of the approximate methods of boundary-layer calculation which were selected, *i.e.*, Thwaites' method (Ref. 2) for the laminar layer and Hewson's method (Ref. 3) for the turbulent layer.

In conclusion it is shown that design methods can be modified to ensure improved performance at a specified Reynolds number or over a range of Reynolds number.

In the course of the report the importance of assessing wind-tunnel results in relation to secondary effects such as the contraction of the air stream in the plane perpendicular to that considered is well illustrated, and methods of correction to enable more universal application of particular results are outlined.

1. *Introduction.*—To allow for the effect of increases of pressure loss occurring in flow through aerofoil cascades at low Reynolds numbers (especially in the case of diffusing flow through compressor-type cascades) present design methods specify in general terms minimum Reynolds numbers below which these high losses are likely to occur and which are, therefore, suggested as giving a lower limit in terms of Reynolds number for the working range. The high losses are usually accompanied by reductions in air deflection and this latter effect lowers further the efficiency of the cascade. Howell's report 'The present basis of axial compressor design' (Ref. 4) which has become, in this country, the standard basis for further work expresses these effects (increased loss and reduced deflection) purely as functions of Reynolds number though the wide scatter of the points from which the appropriate curves are derived suggest that only average values are represented.

The extensive programme of cascade tests, described in Ref. 1, carried out at the Cambridge University Engineering Laboratory over a range of Reynolds number from $3{\cdot}0 \times 10^4$ to $5{\cdot}0 \times 10^5$ has supplied much useful data in this respect. This report represents an attempt to assess results and to produce, in conjunction with theoretical analysis, more accurate means of estimating and predicting the onset and magnitude of high losses at low Reynolds numbers.

2. *Experimental.*—2.1. *Apparatus.*—The low-speed wind tunnel which is fully described in Refs. 1 and 5 and is shown diagrammatically in Fig. 1 is of the open pressure-type, arranged to exhaust to atmosphere on the outlet side of the cascade under test. Three cascades, all of the compressor type, were tested. In each case the individual blade sections were the C.4., profile of the National Gas Turbine Establishment having a thickness/chord ratio of 10 per cent and based on circular-arc camber-lines. The three cascades had camber angles of 20 deg, 30 deg, and 40 deg respectively and the corresponding stagger angles of -34 deg, -36 deg, and -38 deg were chosen to give an outlet angle of approximately 30 deg in each case. The pitch/chord ratio was $1{\cdot}0$ and the actual chord length of the blades was 6 in. To reduce three-dimensional effects as far as possible an aspect ratio of $3{\cdot}0$ was used and in order to simulate the effect of an infinite cascade nine blades were set in each cascade with the end blades merging into the top and bottom walls of the tunnel. To reduce further wall effects a limited amount of boundary layer suction was applied immediately prior to the cascade in the wall leading to the top blade of the cascade (this blade having its suction surface exposed to the flow).

From traverses taken upstream and downstream of the cascade, typical plots of which are shown in Fig. 2, values of mean air deflection, pressure rise, and total-head loss were obtained. The air intake of the wind tunnel was subjected to various degrees of throttling to ensure that conditions of air velocity, etc., remained constant during each test. A static-pressure tapping in the settling chamber of the tunnel was used as a datum for these adjustments and the reading were corrected for any slight variations which did occur in spite of the adjustment obtained by throttling the intake. The close agreement of the total-head pressure values for inlet and outlet traverses outside the wakes, as shown in Fig. 2, confirm the accuracy of the tests. It is worthy of note that no difficulty was experienced in repeating results obtained previously. Forty-four pressure tappings located round the centre-section of the middle blade of each cascade enabled normal-pressure distributions to be plotted. The large number of tappings available, though all forty-four were not used in every test, permitted detailed distributions to be plotted.

In addition to these tests some work was carried out on visual methods of observing the general pattern of the flow. An oil smoke generator of the National Physical Laboratory pattern producing a mist of heated paraffin vapour (Ref. 6) was constructed and observations were made on a thin filament of this smoke introduced into the main stream through a narrow slot in the surface of one of the blades, this slot being located slightly downstream of the leading edge on the suction surface.

A set of model blades corresponding to the 40-deg camber blades was set up in an equivalent cascade and was tested in the electric potential tank at the National Gas Turbine Establishment (Pyestock). The pressure distributions obtained by this method, in comparison with the wind-tunnel distributions, were used as the basis for further calculation and to enable corrections to be made for three-dimensional flows in the tunnel.

2.2. *Presentation of the Results.*—Mention has already been made of the mean values which were calculated and used as the basis for assessing and comparing the results, namely air deflection, pressure rise, and total-head loss. From this data the value of efficiency was calculated as defined by Howell:

$$\text{Efficiency} = 1 - \frac{\text{mean total-head loss}}{\text{theoretical pressure rise}}$$

Plots of efficiency, and air deflection over the full range of Reynolds number for the 40-deg camber cascade at inlet angles of 50 deg and 60 deg are shown in Fig. 3. The calculation of mean values from the traverse figures is discussed in Appendix I.

The use of lift and drag coefficients in presenting the results has been avoided because of errors arising in their estimation from the standard expressions due to varying amounts of three-dimensional flow encountered during the tests.

The theoretical pressure rise is defined as the pressure rise which would be achieved if there were no pressure losses and the same air angles were maintained. The expression is :

$$= \tfrac{1}{2}\rho_1 V_1^2 - \tfrac{1}{2}\rho_2 V_2^2 \quad . \quad . \quad . \quad . \quad . \quad . \quad . \quad . \quad . \quad (1)$$

The normal-pressure distributions have been plotted relative to the prevailing conditions at outlet and on a non-dimensional basis (*see* Figs. 4 and 5). The expression for the ordinate is thus :

$$\frac{\text{local normal pressure} - \text{outlet static pressure}}{\text{outlet velocity head}} = \frac{p - p_2}{\tfrac{1}{2}\rho V_2^2} \quad . \quad . \quad . \quad . \quad . \quad (2)$$

The abscissa is :

$$\frac{\text{distance along chord from leading edge}}{\text{total chord length}} = \frac{x}{C} \quad .$$

This form of non-dimensional plotting enables direct comparison of pressure distributions to be made as, on this scale, the pressure at the leading-edge stagnation point approximates to the value 1·0 (actual value 1·0 in the case of potential flow) and the pressure approaching the trailing edge tends to zero.

3. *Discussion of Results and Comparison With Theory.*—3.1. *Three-dimensional Effects.*—Despite the comparatively large span of the blades of the cascades the effect of the wall boundary layers was very marked when deflections were high. In these cases a noticeable discrepancy was noted in the two-dimensional continuity of the flow at the centre of the cascade span, this being attributed to the thickening of the wall boundary layers accelerated by the pressure rise across the cascade. The increase in displacement thickness of these boundary layers causes the effective area of flow to be reduced and a measure of this effect is given by the contraction coefficient :

$$\xi = \frac{\int \rho_1 V_1 \cos \alpha_1 \, dy}{\int \rho_2 V_2 \cos \alpha_2 \, dy} \quad . \quad . \quad . \quad . \quad . \quad . \quad . \quad . \quad . \quad (3)$$

Representative values of ξ for various cases are given in Table 1, Appendix II, the corresponding cascade, Reynolds number, and deflection being quoted in each case. It is seen that at small deflections ξ is close to unity and the contraction effect is not serious. As the deflection increases ξ falls rapidly, but is not less than 0·9 until deflections of over 20 deg are reached.

The detailed modifications imposed by this effect on the two-dimensional flow are of a complex nature but it is clear that the contraction of the flow in a plane perpendicular to those of the cascade and of the vertical centre-section of the tunnel will cause acceleration of the flow in opposition to the normal diffusing effect of the cascade. The measured pressure distributions do not correspond to those associated with the measured deflections under conditions of true two-dimensional flow ; in particular, adverse pressure gradients are lessened and breakaway tends to be suppressed. Furthermore, the effective Reynolds numbers at positions near the trailing edge are increased above their proper two-dimensional values.

Although the actual planes of traverse are three chord lengths apart the entire pressure rise effectively takes place over the cascade itself. It is clear that most of the increase in the thickness of the wall boundary layers must also occur within the cascade. This has been confirmed

by traverses taken over the whole area of flow within half-a-chord length of the cascade. A simple correction has been devised to the two-dimensional potential flow pressure distributions. This assumes that all the contraction does take place across the cascade itself and that the increase of boundary-layer displacement thickness along the wall can be expressed as a simple function of the distance along the chord line from the leading edge.

The derivation of this correction is given in Appendix III and the result only is quoted here. If the suffix $[\ ]_{\xi=1}$ refers to conditions which would obtain with true two-dimensional flow, then :

$$\frac{[p]_{\xi=1} - [p_2]_{\xi=1}}{\frac{1}{2}\rho[V_2]^2_{\xi=1}} = 1 + \frac{1}{\xi^2}\left[1 - (1-\xi)\left(\frac{x}{C}\right)^n\right]^2\left[\frac{p - p_2}{\frac{1}{2}\rho V_2^2} - 1\right] \quad \ldots \quad \ldots \quad \ldots \quad \ldots \quad (4)$$

where p is the local normal pressure at a point on the surface of one of the aerofoils, and the displacement thickness of the wall boundary layer through the cascade is assumed to increase as the function $(x/C)^n$.

It is to be expected that such a simple assumed form for the wall boundary-layer growth produces a certain amount of distortion in the corrected distribution, but it should be realised that the correction is only important when the contraction is considerable ($\xi < 0{\cdot}9$). Large contractions occur only when high deflections are involved and, in turn, these arise at high positive incidences. Under these conditions the pressure distributions for all three cascades are of similar form. The form of the pressure distribution must determine the growth of the wall boundary layers. From the above argument it would seem reasonable that, when the contraction is large and the correction in pressure considerable, the value of the power in the above expression which gives the closest approximation for one cascade would also give a good approximation for the other cascades. The value $n = 3{\cdot}0$ was found to give the best results for these tests. The potential-flow pressure distributions in their original form and also when corrected to three-dimensional flow using the experimental values for ξ have been compared with the tunnel distributions in Figs. 4 and 5. In each case the wind-tunnel distribution at the highest inlet Reynolds number has been shown, since under these conditions boundary-layer thicknesses on the blade surface are small and will only cause slight modification to the potential-flow distribution. Agreement is good, the discrepancy towards the trailing edge on the suction surface in the case of the 40-deg camber cascade at $\alpha_1 = 60$ deg being largely the result of turbulent separation affecting the wind-tunnel distributions.

The wind-tunnel distributions could have been corrected to two-dimensional conditions but this would be misleading in that the observed boundary-layer characteristics would no longer correspond to the higher pressure gradients of the modified distribution.

The contraction effect reduces the static-pressure rise from that corresponding to the measured deflections and the extent of this discrepancy is indicated in Figs. 6 and 7. The expressions from which these curves have been derived are obtained in Appendix IV. In some cases the pressure rise is reduced by as much as 40 per cent. Therefore in any general interpretation of results the contraction ratio should be specifically stated together with the presentation of relationships between efficiency and deflection though this difficulty does not arise if pressure distributions themselves are taken as the basis for comparison.

The increased thickness of the boundary layers on the walls of the tunnel leads to a loss of lift round the sections of each blade adjacent to the walls and this effect in turn gives rise to secondary flows which can be represented as a series of vortices. These effects greatly increase the losses but do not modify the flow at the centre-section to the same extent as the contraction effect mentioned above. Secondary flows in this cascade tunnel have been the subject of a separate investigation (Ref. 7). At the highest incidences, appreciable secondary flows were detected and in the case of the 40-deg camber cascade at $\alpha_1 = 60$ deg, traverses were taken over the entire outlet area. These traverses were taken half-a-chord length downstream of the cascade. The variation of outlet angle and mean total-head loss across the section are shown in Fig. 8.

Although it is clear that the flow near the walls is seriously affected, only the effect on the two-dimensional flow at the centre-section need be considered in this report. The value of the mean total-head loss at the centre-section is virtually unaltered but the effective incidence angle is reduced. Using the relations given in Ref. 8, the reduction of incidence in the case considered above is slightly less than 2 deg. The secondary flows in this case were the most extensive encountered in the whole series of tests so that it may safely be assumed that induced effects were correspondingly less in the other cases. As with the pure contraction effect this secondary flow does not materially affect the interpretation of results in this work as pressure distributions are used as the basis for comparison.

3.2. *Potential Flow.*—In the case where the actual cascade is given and it is required to predict the potential flow, the electric potential tank method is probably the most satisfactory since it is much more rapid than computational methods and can give the same degree of accuracy. Pressure distributions obtained from tests in the electric tank are compared with the corresponding wind-tunnel distributions for the 40-deg camber cascade in Figs. 4 and 5. As mentioned in the previous section, the use of the three-dimensional correction is also illustrated. The Joukowski condition, *i.e.*, location of the rear stagnation point on the trailing edge, was used to determine the value of the circulation and thus the outlet angles in the electric tank. Since the wind-tunnel distributions are modified by the existence of boundary layers on the surfaces of the individual blades, it would clearly be more correct to calculate the potential flow past a series of aerofoils based on the original sections but with the displacement thickness of the boundary layer added on all the way round. However, this would involve complete recalculation of the potential flow for each Reynolds number and the arithmetical work would have been increased enormously. At high Reynolds numbers, where the displacement thickness of the boundary layer is small, agreement is good, even when the contraction ratio is comparatively large, provided that the correction is applied.

3.3. *The Laminar Layer.*—In virtually all cases in the wind-tunnel tests, as the Reynolds number is reduced, rising pressure gradients on the pressure distributions are interrupted. This effect which is the primary cause of the rapid falling-off in efficiency is due to the onset of laminar breakaway.

Comparison of the three cascades at varying incidences shows that the Reynolds number at which the efficiency is seriously affected varies considerably, thus suggesting that certain types of pressure distributions give rise to better low-speed characteristics than others. In the laminar layer only a very limited rise in pressure can be achieved before the separation point is reached and the large pressure rises occurring on the suction surfaces of the aerofoils take place mainly in the regions where the boundary layer is in the turbulent form, *i.e.*, after transition. If transition to turbulent flow takes place before the laminar separation point is reached, separation of the laminar layer will not occur and the local pressure rise will be maintained. If the transition point moves back towards the trailing edge, as would result from a reduction of the inlet Reynolds number, separation will begin but will be arrested soon after the transition point when the boundary layer returns to the surface in the turbulent form. Further movement of the transition point in a rearward direction allows separation to develop before the subsequent recovery in the turbulent layer and, finally, a stage is reached at which breakaway is complete before transition resulting in no further rise of static pressure. The nature of the return to the surface of a separated layer is not fully understood but it is certainly affected by the curvature of the surface of the aerofoil and hence the curvature of the air stream adjacent to the surface. With a convex surface, as is encountered on the suction side of the aerofoil, there must be a rising static pressure away from the surface to balance the centrifugal forces caused by the curvature of the stream. This rising pressure will clearly help to force a separated layer back to the surface. However, the return of the flow to the surface will not take place until transition has occurred and the curvature as such does not affect the value of the Reynolds number at which local breakaway first occurs.

This is the explanation of the hump in the pressure-distribution curves at the lower Reynolds number. This hump represents the ' bubble of turbulence ', which is separation of the laminar layer followed by transition and the return of the turbulent layer to the surface, enclosing a ' dead ' region adjacent to the surface. The above explanation shows why this hump grows larger as the Reynolds number is decreased until ultimately the breakaway is complete and no further rise of pressure is observed. Examples of separation are seen in the pressure distributions shown in Figs. 10 and 11, the corresponding cascade, incidence, and Reynolds number being indicated on the curves. Qualitative observations using the smoke technique as described previously have confirmed these deductions showing distinctly three phases of change with increasing Reynolds number, *i.e.*, complete breakaway, local breakaway enclosing a bubble of turbulence and, at the higher air speeds, smooth uninterrupted flow in the turbulent boundary layer adjacent to the surface.

A full description of Thwaites' approximate method of laminar boundary-layer calculation is given in Ref. 2, but a brief outline will be given here. The method is developed from the von Kármán momentum equation and the final equations are thus given in terms of the displacement and momentum thicknesses of the boundary layer. Thwaites uses the known solutions of a number of particular cases and, from a mathematical approach, derives a general solution which fits all these cases and is of relatively simple form. In the final approximate form Thwaites gives :

$$\theta^2 = \frac{0{\cdot}45\nu \int_0^s V_\delta^5 \, ds}{V_\delta^6} \qquad \ldots\ldots\ldots\ldots\ldots\ldots\ldots\ldots \quad (5)$$

$$m = -\frac{\theta^2}{\nu}\frac{dV_\delta}{ds} \qquad \ldots\ldots\ldots\ldots\ldots\ldots\ldots\ldots \quad (6)$$

where θ is the boundary-layer momentum thickness

s is the distance along the surface from the forward stagnation point

V_δ is the local velocity in the main stream at the edge of the boundary layer

ν is the kinematic viscosity

m is the form parameter of the velocity distribution across the boundary layer.

The suffix 0 refers to conditions at the forward stagnation point. Thwaites also gives : $m = 0{\cdot}082$ at separation.

From the above it is seen that

$$m = -\frac{0{\cdot}45 \int_0^s V_\delta^5 \, ds}{V_\delta^6}\frac{dV_\delta}{ds} \qquad \ldots\ldots\ldots\ldots\ldots\ldots\ldots\ldots \quad (7)$$

and is dimensionless. The value of m at each point of the surface for a pressure distribution plotted non-dimensionally as in this report, is unique and independent of the absolute magnitude of the velocity. This implies that the point at which m reaches the value $0{\cdot}082$, *i.e.*, the separation point, is determined only by the form of the non-dimensional pressure distribution and is independent of the Reynolds number. This deduction appears to agree with the experimental evidence, in that the laminar-separation point does not move appreciably with changing Reynolds number as long as the experimental velocity distribution remains close to the potential-flow distribution.

Values of m along the suction (convex) surfaces of the blades have been calculated in a number of cases ; examples of the calculated values are shown graphically in Fig. 12. The velocity distributions used to supply the numerical data were those obtained in the wind tunnel at

Reynolds numbers of approximately $5 \cdot 0 \times 10^5$ and $2 \cdot 1 \times 10^5$ respectively, though the potential flow distributions were also used in the case of the 40-deg camber cascade. The predicted laminar separation points (where $m = 0 \cdot 082$) agreed well with the separation points obtained in the tests, either by estimation from the hump in the pressure distribution or by visual observation using smoke filaments.

As was mentioned earlier, the laminar-separation points only remain unaffected by changes of Reynolds number so long as the pressure distributions remain sensibly unaltered but it is clear that this is no longer the case when the Reynolds number becomes very small. The actual change in the pressure distribution is exaggerated by the method of non-dimensional plotting, in which pressures are represented as proportions of the outlet velocity head since reduced suction pressures at low Reynolds numbers give rise to reduced deflections and cause relative increases in the outlet velocity and hence in the velocity head ; thus the ratio $(p - p_2)/\frac{1}{2}\rho V_2^2$ is reduced in an exaggerated proportion. A truer picture of the actual changes in the pressure distribution is obtained if the pressures are plotted as proportions of the inlet velocity head and an example of this method of plotting is shown in Fig. 13. As will be seen the changes in the shape of the curves up to and after the separation point due to changes of Reynolds number are still considerable. These changes are due to the actual breakaway of the laminar layer and also to the increase of displacement thickness all over the surface. From the potential flow aspect these effects correspond to a general increase in the thickness of the basic aerofoil shape which is particularly marked after the separation point, and a decrease in the magnitude of the circulation. The forward movement of the forward stagnation point due to loss of circulation is very small and is certainly insufficient to justify alteration of the datum point for the calculation of m.

Equation (5) indicates that for similar pressure distributions the momentum thickness is inversely proportional to the square root of the velocity (inlet Reynolds number). The ratio $\sqrt{(V_{max}/V_1)}$ is equal to the corresponding ratio $\frac{\theta \text{ at Reynolds number considered}}{\theta \text{ at maximum Reynolds number}}$ (where maximum Reynolds number is in this case $5 \cdot 0 \times 10^5$) and is plotted against Reynolds number in Fig. 14. It is seen that, for similar pressure distributions, when the Reynolds number falls to $2 \cdot 2 \times 10^5$ the momentum thickness is only $1 \cdot 5$ times as large, whereas the corresponding magnification for Reynolds numbers of $1 \cdot 0 \times 10^5$ and $0 \cdot 3 \times 10^5$ are $2 \cdot 2$ and $4 \cdot 0$ respectively. Since increases of momentum thickness and hence of displacement thickness will modify the potential-flow distribution, the accurate calculation of θ would involve a step-by-step process giving finally values of θ somewhat less than those indicated above. However this further readjustment of θ is not likely to be large and will certainly not affect the general form of the curve, which shows that rapid changes in the displacement thickness can be expected at the lower Reynolds numbers. The proportionate increase in θ will affect the pressure in a somewhat similar way to the three-dimensional contraction of the flow. In particular, pressure gradients will be reduced especially as the separation point is approached. The value of m, which is a linear function of the velocity gradient, will therefore be reduced and the separation value ($0 \cdot 082$) will occur at a point further downstream than the original separation point.

The other factor causing the pressure distribution to alter with changing Reynolds number, the loss in circulation, is fundamentally a result and not a cause of laminar breakaway and cannot therefore play any part in determining whether or where laminar separation will occur. It is sufficient therefore to consider only the original pressure distribution together with the correction for the change of θ.

What actually causes the experimental distributions to assume their final form can best be understood by imagining in the first place that the circulation is maintained and that the pressure distribution is that corresponding to potential flow with the displacement thickness added on to the basic shapes. Laminar separation will then take place at the point at which m reaches the value $0 \cdot 082$ and further changes in the distribution will result from the decrease in circulation and the existence of a region of reverse flow adjacent to the surface and immediately following

the separation point. The estimation of such large changes in the pressure distribution (*i.e.*, where extensive laminar separation occurs) from the potential flow figures would be extrernely complicated, if at all possible, and would be, in any case, of only academic interest since efficiencies would have reached impracticably low values.

It will be appreciated that the performance of cascades at low Reynolds numbers is almost entirely determined by the relative positions of the laminar separation and transition points. For this reason further discussion of laminar separation would be futile without previous consideration of the factors affecting transition.

3.4. *Transition.*—That transition does not, in fact, occur suddenly at a definite point but develops through a region may appear to render reference to a transition point meaningless but it is nevertheless convenient to consider transition as occurring suddenly at a point. This somewhat artificial conception can be justified if the point is regarded as the effective centre of the region. A definition of the mean transition point is given in Ref. 9.

The mathematical approach to the problem of transition has so far been limited to a study of the amplification of small disturbances in the laminar layer. The work of Schlichting in this connection (Ref. 10) has had notable success in its agreement with experiment (Ref. 11) but this approach has not yet reached the stage at which prediction of actual transition points in flows where pressure gradients are present may be undertaken. However, this theory and the fact that the change to turbulent flow appears to be gradual rather than a sudden occurrence do suggest that transition is not merely a function of velocities and boundary-layer thicknesses at a particular point but is determined by the development of the boundary layer over a considerable part of the surface.

Transition measurements made by Preston, Sweeting and Brown (Ref. 9) on single aerofoils in a low-speed wind tunnel at the National Physical Laboratory together with other miscellaneous transition data were studied in great detail with a view to obtaining a better understanding of the factors promoting transition. The forward movement of the transition point along the surface with increasing inlet velocity (Reynolds number) is well known but it is also evident from the results considered, that the pressure gradient is itself an important factor in determining transition. In particular large positive pressure gradients accelerate the process of transition whilst negative pressure gradients extend the region of laminar flow and cause the transition to turbulent flow to be more gradual when it eventually does take place. These very general deductions give no practical assistance in the matter of determining actual transition points but are nevertheless of great help to qualitative analysis of the results especially in conjunction with the work on the laminar layer.

It is now possible to consider in greater detail the relationship between laminar breakaway and transition at low Reynolds numbers. At high positive incidences (but still below the critical value) the pressure distributions have, on the convex suction surface, a sharp suction peak located close behind the leading edge. As the incidence is reduced this peak becomes more rounded and moves back towards the trailing edge (*see* Fig. 9). If the peak is too sharp and is followed by an excessively steep pressure gradient, *i.e.*, above the critical incidence, efficiencies fall rapidly. Thus it appears that pressure distributions with a moderately sharp suction peak near the leading edge on the convex surface are likely to give the best overall performance at low Reynolds numbers.

This conclusion can also be reached from theoretical considerations. In the expression given for m in equation (7) the velocity gradient corresponding to the separation value of 0·082 increases as the $\int V_\delta^5 \, ds$ term grows smaller. Separation will not occur until the pressure begins to rise (*i.e.*, after the suction peak) so that as this peak moves back along the surface the value of the integral $\int V_\delta^5 \, ds$ up to this position increases and separation will subsequently occur in correspondingly smaller pressure gradients, and the actual rise in pressure from the point of

maximum velocity (suction peak) will be reduced. At the other end of the scale it is clear that when the pressure gradient becomes very large, as with excessively high incidences, separation will occur even though the $\int V_\delta^5\, ds$ term is still relatively small. From the conclusions reached in respect of transition it will be realised that an appreciable pressure rise before the separation point will be beneficial in that it will promote early transition and so tend to create a turbulent layer before the theoretical laminar-separation point is reached. The type of pressure distribution which permits an appreciable pressure rise before the laminar-separation point is, in fact, of the form suggested earlier, *i.e.*, having a sharp suction peak close to the leading edge and it is significant that this type of distribution offers a further advantage in respect of low-speed performance. This advantage arises from the considerable rearward movement of the separation point due to the increase of displacement thickness at low speeds, a factor which tends to reduce pressure gradients over the front portion of the aerofoil but has considerably less effect on the $\int V_\delta^5\, ds$ term. This latter point is illustrated in Fig. 15 in which the positions of the laminar separation points over the range of Reynolds numbers for representative peaked and rounded distributions are plotted. These are for the 20-deg camber cascade at $\alpha_1 = 50$ deg and 40-deg camber cascade at $\alpha_1 = 50$ deg respectively.

No mention has so far been made of the effects on the concave (pressure) surfaces of the blades. Large pressure rises do not normally occur on these surfaces and thus laminar breakaway will not take place except at high negative incidences. However, in the case of the 40-deg camber cascade at $\alpha_1 = 35$ deg there was evidence of local separation taking place shortly after the suction peak on the concave surface at the maximum Reynolds number but the effect disappeared as the Reynolds number was reduced. The disappearance of laminar separation at lower Reynolds numbers does not, in fact, contradict previous conclusions since it was found to be caused by increases in boundary-layer thickness and loss in circulation causing general reduction of pressure gradients.

3.5. *The Turbulent Boundary Layer.*—It is in the region of the turbulent boundary layer that most of the pressure recovery along the surface from the suction peak must take place and, since the diffusing cascade is inevitably associated with high pressure gradients, it is obvious that the turbulent layer represents an important factor in the performance of the separate aerofoils of the cascade and thus of the cascade as a whole.

Two particular features of the turbulent boundary layer are of significance in this type of flow, namely :

(*a*) Turbulent layers can remain in contact with the surface against considerable rises in static pressure, though not indefinitely.

(*b*) The skin-friction coefficients in the turbulent layer are much higher than those in the laminar layer.

That there is a definite limit to the total pressure rise which can be obtained in the turbulent layer is shown by certain of the experimental results in which there is evidence of turbulent separation occurring near the trailing edge. One such case is the 30-deg camber cascade at $\alpha_1 = 60$ deg in which the pressure distribution (Fig. 10) is noticeably affected at the higher speeds, the separation effect being shown up by a flattening out of the pressure rise on the suction surface towards the trailing edge. The associated efficiency curve has a definite peak at a Reynolds number of $3{\cdot}0 \times 10^5$ and thereafter turbulent separation causes increased losses in addition to the gradual increase of skin-friction loss which is discussed later in the report. It may be imagined that turbulent separation, which is commonly referred to as stalling, is purely a high Reynolds number phenomenon for a given incidence but it will be shown subsequently that under certain conditions turbulent separation can reappear at low Reynolds numbers.

Whereas a few exact solutions have been obtained for flow in the laminar layer and reasonably accurate and workable methods have been devised for the general case, the mathematical approach to the more complex flow in the turbulent layer has reached a less advanced stage. Some of the approximate theories for the turbulent boundary layer are discussed in Appendix V and reasons are given for the choice of Hewson's method in this work.

The two forms of Hewson's approximate equation are:

$$\frac{\theta}{\theta_0} = \left[1 + \frac{sT_0}{2}\left(3\frac{V_\delta}{V_0} - 1\right)\right], \quad \ldots \quad (9)$$

and

$$\frac{\theta}{\theta_0} = \left[1 + 1{\cdot}133T_0 \int \left(\frac{V_\delta}{V_0}\right)^{1{\cdot}133(H+2)} ds\right]^{0{\cdot}882} \left(\frac{V_\delta}{V_0}\right)^{-(H+2)}, \quad \ldots \quad (10)$$

the first equation being an approximate form of the second. These equations apply up to a critical point which is defined as the point at which $d\theta/ds$ reaches the value $0{\cdot}01$ and which indicates the beginning of the region in which the pressure difference across the boundary layer itself becomes significant. The critical point is reached before separation proper but it is clear that any appreciable pressure difference across the boundary layer will reduce the normal pressure at the surface and cause increases in the form drag.

$\theta_0 T_0 = (\tau/\frac{1}{2}\rho V^2)_0$ is calculated from the Squire and Young friction law for turbulent layers (the suffix 0 referring to conditions at the beginning of the turbulent layer, *i.e.*, immediately after transition),

i.e.,

$$\theta_0 T_0 = \frac{1}{(5{\cdot}89 \log_{10} 4{\cdot}075 R\theta)^2} \quad \ldots \quad (11)$$

where $R\theta$ is based on the momentum thickness and local velocity at the edge of the boundary layer.

From these equations it can be seen that the development of the turbulent layer is greatly affected by conditions immediately after transition. If θ_0 increases, the turbulent layer develops more rapidly, the critical point is reached sooner and the point of breakaway also moves forward. The variation of $R\theta$ likely to be encountered is summarised in Appendix VI. It is clear that extension of the laminar layer by delayed transition will have an adverse effect on the turbulent layer since the value of θ_0 is increased and, for the same pressure rise from the suction peak, pressure gradients in the turbulent layer must be increased to compensate for reduced gradients in the laminar layer.

These effects act not only as the result of changes in the basic pressure distribution but are also influenced by varying Reynolds number. Whereas, at reduced Reynolds numbers, the starting point of the turbulent layer is moved towards the trailing edge, the value of θ at transition increases and the distance between the commencement of the turbulent layer and the critical point is smaller. These two factors act in opposition and although a decrease in Reynolds number from the maximum value will cause the critical point to move rearwards along the surface as the speed continues to fall the increase in the value of θ_0 will overcome this effect and cause the critical point to move forwards again. This latter condition is usually obscured by the onset of laminar separation but is of importance in cases where the laminar-layer characteristics are favourable.

Detailed calculations on the turbulent layer have been made and some of the results are shown graphically in Figs. 16 and 17. Fig. 16 shows the growth of the momentum thickness along the surface for the 30-deg camber cascade at $\alpha_1 = 60$ deg and at Reynolds numbers of $5{\cdot}1 \times 10^5$ and $0{\cdot}95 \times 10^5$ and the critical gradient $d\theta/ds$ is also indicated. Both the Hewson formulae were used in a number of the calculations but the differences in the resulting values of $R\theta$ were slight.

The modified Hewson equations covering the region after the critical point and up to separation have been described briefly in Appendix V and have been applied where possible to these results. On Fig. 17 the relative positions of the critical and separation points, as calculated by this method, are compared. The considerable distance between the critical point and separation should be noted. It is significant that the experimental pressure distributions show

first signs of irregularity at positions roughly midway between these two points. Unfortunately neither the position of the critical point nor that of the separation point presents a direct criterion for the beginning of a region of high loss but it would appear that adverse effects are negligible if the critical point is fairly near to the trailing edge (say within 0·2 chord length) provided that pressure gradients in that region are not excessive. If the calculated positions of turbulent separation, shown in Fig. 17, are marked on the pressure distributions in Figs. 9 and 10, it will be seen that at the highest Reynolds number fairly good agreement was obtained between the calculated and actual separation points.

3.6. *Skin Friction in the Laminar and Turbulent Layers.*—Accurate estimation of the form drag from integration of the normal-pressure distribution projected along the vector mean direction is difficult at the higher Reynolds numbers when the form-drag coefficient becomes extremely small. Furthermore, the difficulty mentioned in section 2·2 in connection with three-dimensional flow effects prohibits the use of the standard expressions when these effects are present. However, consistent values for both the total-drag and form-drag coefficients were obtained in a number of cases and the difference of these two coefficients gives a reasonable indication of the magnitude of the component due to skin friction. Typical values of the coefficients plotted against Reynolds number are shown in Fig. 18.

Since transition points move forward along the surface as the Reynolds number is increased, the total extent of the turbulent layer increases. In addition to this, since skin friction in the turbulent region is invariably greater than in the laminar layer, the skin-friction coefficient may be expected to increase with Reynolds number. This effect is apparent on Fig. 18 in which the skin-friction coefficient is equal to the difference in the ordinates of the two curves at a given Reynolds number. It is interesting also to compare the relative magnitudes of this component of the drag for different types of pressure distribution. The type of distribution occurring at high positive incidences is associated with large skin-friction coefficients because transition occurs nearer the leading edge and also because mean square velocities on the suction surface are higher.

Although the skin-friction drag has little significance at low Reynolds numbers it is of as much importance as the form drag at higher air speeds where the efficiency reaches its maximum. Once the Reynolds number is high enough to prevent the occurrence of laminar breakaway the advantage of high incidence and the resulting position of the suction peak near the leading edge is largely offset by the relatively large value of the friction drag, although the form drag can become very small as in the case of the 20-deg camber cascade at $\alpha_1 = 50$ deg (Fig. 18).

3.7. *Pressure Distribution and Performance.*—Whilst the skin-friction drag in the laminar layer is a definite source of loss in this type of flow it, nevertheless, forms only a small proportion of the total loss. The experimental values show that in all cases when transition occurs late (at the lowest Reynolds number) and the laminar layer is maintained over a large part of the surface the friction drag is extremely small. Thus the increase of friction drag as transition moves forward must all occur in the turbulent layer since the extent of the laminar layer is actually decreasing. This is in agreement with well-established data on friction drag in laminar and turbulent layers. The skin-friction coefficients for the laminar layer represent optimum values and, since this analysis is mainly concerned with reduction of losses, laminar skin friction will not be considered in further detail and cascade performance will be assessed in relation to three main factors namely: laminar separation, turbulent separation and skin friction in the turbulent layer.

Laminar breakaway occurs in all the cases covered by these tests provided the Reynolds number is low enough. It will only occur in positive pressure gradients, but since these are unavoidable in diffusing cascades it may be assumed that separation of the laminar layer must take place at some low value of the inlet Reynolds number with cascades of this type. The experimental results have shown that the development of laminar separation causes very large increases in the total loss and the efficiency falls to values well below practical limits of usefulness.

Turbulent breakaway can have similar serious effects on cascade performance. Although extensive turbulent breakaway did not occur during the tests on which this report is based, at even higher incidences very extensive turbulent breakaway takes place, this phenomenon being commonly referred to as ' stalling '. It is significant, however, that in such extreme cases, where turbulent separation occurs at a considerable distance from the trailing edge, large changes of Reynolds number do not effect any material change (*i.e.*, the movement of the turbulent separation point along the surface is not large). This effect agrees with the theoretical calculations, the results of which are plotted on Fig. 17. Severe turbulent breakaway may therefore be regarded as limiting the incidence rather than the Reynolds number, though it will be shown later that improved blade shapes can delay the effect.

In cases where turbulent separation is just beginning near the trailing edge the resulting loss is less serious and may only cause a drop of 1 or 2 per cent in efficiency. Under such circumstances the movement of the turbulent separation point over the Reynolds number range, though small, will be significant and will be responsible for limiting the maximum efficiency and determining at what Reynolds number it occurs.

The effect of turbulent skin friction in limiting the performance can be regarded as of somewhat similar order to that of partial turbulent separation.

It has been shown in section 3.4 that the moderately peaked pressure distributions resulting from positive incidence angles give better characteristics at low Reynolds numbers by inducing transition to occur before the laminar separation point has been reached (compare pressure distributions and efficiencies for the 40-deg camber cascade at $\alpha_1 = 50$ deg and $\alpha_1 = 60$ deg, Figs. 3 and 9). It should be noted that there is a definite limit to improvement by this means as above a certain critical incidence laminar breakaway is again encountered, occurring very suddenly near the leading edge even at the higher Reynolds numbers, as with the 20-deg camber cascade at $\alpha_1 = 60$ deg.

In cases where the negative pressure at the suction peak is appreciable, the total pressure rise from the suction peak to the trailing edge is considerable and the majority of this pressure rise must still take place in the turbulent part of the boundary layer. For this reason and because the turbulent layer covers a larger proportion of the surface, due to earlier transition, losses in the turbulent region are increased. In cases where the maximum suction pressure is excessive, turbulent breakaway either occurs or is closely approached near the trailing edge at high Reynolds numbers (40-deg camber, $\alpha_1 = 60$ deg ; 30-deg camber, $\alpha_1 = 60$ deg ; 20-deg camber, $\alpha_1 = 55$ deg). Under these circumstances the form drag again begins to increase and although this increase is only marked in the case of the 30-deg camber cascade at $\alpha_1 = 60$ deg considerable increases of drag would occur in the other cases quoted above if the Reynolds number were increased still further or if a higher degree of turbulence were present in the inlet stream. It is clear therefore that in most cases there is an optimum Reynolds number at which the maximum efficiency is obtained. This is clearly indicated with the 30-deg camber cascade at $\alpha_1 = 60$ deg and 55 deg, the optimum Reynolds numbers for these cases being $2{\cdot}8 \times 10^5$ and $4{\cdot}1 \times 10^5$ respectively. In the $\alpha_1 = 60$ deg case for this cascade the efficiency drops from 95·4 per cent to 92·4 per cent as the Reynolds number is increased from the optimum value of $2{\cdot}8 \times 10^5$ to the maximum test value of 5×10^5, the form drag rises sharply. This is anticipated by the theory, which predicts that turbulent separation will occur at 0·15-chord from the trailing edge. The effect of separation on the pressure distribution is well defined.

It has been suggested previously that, if separation of the turbulent layer is to be avoided, the total pressure rise from the suction peak must not exceed a certain value, and since the positioning of this peak near the leading edge is essential for good low Reynolds number characteristics, this implies a limitation on the maximum lift possible if reasonable efficiencies are to be maintained over a wide range of Reynolds number. It is interesting to note, however, that small differences in the pressure distribution can have an appreciable effect on performance

and may lead to increases in the maximum permissible lift. This is well illustrated by comparison of the pressure distributions at the highest Reynolds number for the 20-deg camber cascade at $\alpha_1 = 50$ deg, the 30-deg camber at $\alpha_1 = 55$ deg, and the 40-deg camber at $\alpha_1 = 60$ deg. The actual pressure rises expressed as a proportion of the inlet velocity head ($\Delta p/\frac{1}{2}\rho V_1^2$) for the three cases are 0·415, 0·348 and 0·336 respectively, the corresponding efficiencies being 96·5 per cent, 95·6 per cent and 95·9 per cent respectively. The pressure rise from the suction peak to the trailing edge as a proportion of $\frac{1}{2}\rho V_1^2$ is practically the same in each case, the actual values being 1·72, 1·58 and 1·69, but it is seen that the development of the turbulent layer is far from identical. In the above three cases there is no indication of turbulent separation with the 20-deg camber cascade (*see* Fig. 11), nor on the 30-deg cascade, but it has occurred in the 40-deg cascade. It is also clear from the pressure distributions that laminar breakaway is less serious at low Reynolds numbers in the 20-deg camber case and this is reflected in the efficiency curves. The superior performance of the 20-deg camber cascade apparent at both ends of the Reynolds number range (efficiency at $\alpha_1 = 50$ deg is 94 per cent at a Reynolds number of $0{\cdot}8 \times 10^5$ rising to 96·5 per cent at 5×10^5) is caused by the steep pressure gradient immediately after the suction peak (Fig. 11) permitting more of the total pressure rise to take place in the laminar layer and allowing the pressure gradient to be gradually reduced as the trailing edge is approached. The full significance of this detail in the form of the pressure distribution will be made clear later in this section when the optimum form is considered.

Turbulent skin friction is more difficult to assess and there is no ready method of estimating its value in any particular case. The advantage of the suction peak near the leading edge in promoting early transition and delaying the onset of laminar breakaway will be partially offset at higher Reynolds numbers on account of the increased loss due to skin friction in the turbulent layer. To a certain extent this effect seems unavoidable but some improvement is possible if high local velocities are not reached after the transition point. The possibility of reducing the actual skin-friction coefficients as given by the Squire and Young law (equation (11)) offers further opportunity for reduction of this loss but the value of $Rn\theta$ at transition for the different cascades at a particular inlet Reynolds number does not show a very wide variation. It seems likely that an attempt to increase its value, and thereby reduce the skin friction at the beginning of the turbulent layer might ultimately increase the possibility of turbulent breakaway. Appreciable reduction of skin-friction loss appears feasible only in cases where performance at low Reynolds numbers is not important and the transition point need not occur near to the leading edge.

4. *Velocity Distributions.*—4.1. *Derivation of Optimum Velocity Distributions.*—To supplement the conclusions reached earlier on a qualitative basis regarding the most favourable form of velocity distribution for particular and specified working conditions it is clearly desirable that quantitative relations should be established. Unfortunately the previous analysis of both laminar and turbulent flows cannot be applied to enable estimates to be made of theoretical distributions unless transition points can also be predicted with some degree of accuracy. The necessary mathematical data for predicting transition is not, at present, available so that in the general case the qualitative conclusions cannot be improved upon,

However there are two special forms of velocity distribution which are worthy of special study and which being themselves determined precisely by mathematical relationships may be of considerable assistance in providing exact datum lines for the synthesis of practical distributions. These two special cases are referred to as the ' Ideal ' forms for the velocity distributions in the regions of the laminar and turbulent layers respectively and represent the distributions which permit the maximum pressure rise from the suction peak to the trailing-edge stagnation point without the possibility of breakaway occurring at any Reynolds number.

4.2. *Ideal Form for the Velocity Distribution in the Laminar Layer.*—According to the approximate theory of Thwaites laminar separation will not occur until the parameter m reaches the value 0·082 so that separation can be avoided altogether, if m never attains this value. If

a distribution is derived in which m is maintained at a constant safe value (slightly less than 0·082) throughout, separation will not occur and, furthermore, the maximum pressure rise will be obtained. This latter condition can be verified if a short section of length ds is considered, at some position on the surface over which the pressure gradient can be assumed constant. The value of $\int_0^s V^5\,ds$ and of V at this section will be determined by the previous form of the distribution and the maximum pressure gradient (a unique function of the velocity gradient) will be attained if m has its maximum permitted value. Thus the maximum pressure rise over the short section is achieved if m is maintained at its highest permitted value; this same argument applies at every point along the surface so that the sum of the pressure rises over a large number of short sections (the total pressure rise) will be a maximum if m is kept constant at the chosen safe value.

It is interesting to find the maximum pressure rise which can be obtained under these conditions and thus to investigate the possible limit of improvement in low-speed characteristics which can be achieved by inducing early transition without any corresponding forward movement of the separation point.

These conditions are likely to be fulfilled in the case in which m remains constant at some safe value slightly less than 0·082. The derivation of mathematical expressions for this particular form of velocity distribution is given below.

Then

$$0{\cdot}45\frac{dV}{ds}\frac{\left[\int_b^s V^5\,ds + X_1\right]}{V^6} = -m' \qquad \ldots\ldots\ldots\ldots\ldots\ldots \quad (12)$$

where $X_1 = \int_0^b V^5\,ds$ and m' is the constant value for m, so that

$$\int_b^s V^5\,ds + x_1 = \frac{-m'\,V^6}{0{\cdot}45\dfrac{dV}{ds}}$$

Differentiating with respect to s

$$V^5 = \frac{-6m'V^5}{0{\cdot}45} + \frac{\dfrac{m'V^6}{0{\cdot}45}\dfrac{d^2V}{ds^2}}{\left(\dfrac{dV}{ds}\right)^2}$$

or

$$1 = \frac{-6m'}{0{\cdot}45} + \frac{m'V\dfrac{d^2V}{ds^2}}{0{\cdot}45\left(\dfrac{dV}{ds}\right)^2}.$$

Thus

$$\frac{0{\cdot}45 + 6m'}{m'}\left(\frac{dV}{ds}\right)^2 - V\frac{d^2V}{ds^2} = 0$$

so that

$$\frac{d}{ds}\left(V^{-r}\frac{dV}{ds}\right) = 0. \qquad \text{where } r = \frac{0{\cdot}45 + 6m'}{m'}$$

and, on integration $V^{-r}\frac{dV}{ds} = A$

where A is a constant.

Thus $\frac{dV}{V^r} = A\,ds$

Integrating $-\frac{1}{(r-1)}V^{-(r-1)} = A.s + B$

where B is another constant.

Thus $V^{-(r-1)} = -(r-1)(A.s + B)$ .. .. (13)

and the general solution is

$$V = \frac{1}{(Ds + E)^{1/(r-1)}} \quad .. \quad .. \quad .. \quad .. \quad .. \quad .. \quad .. \quad .. \quad (14)$$

the two constants D and E being determined by the boundary conditions.

From equation (14) above

$$\frac{dV}{ds} = \frac{-D(Ds + E)^{-r/(r-1)}}{(r-1)}$$

$$= \frac{-DV}{(r-1)(Ds + E)} \quad .. \quad .. \quad .. \quad .. \quad .. \quad .. \quad .. \quad .. \quad (15)$$

Assuming that $V = V_{max}\,(s/b)^{1/4}$ from s = 0 to the suction peak where $s = b$,

then $x_1 = \int_0^b V^5\,ds = 0{\cdot}4444V_{max}{}^5 b.$

But, since $m' = -0{\cdot}45\,\frac{\int V^5\,ds}{V^6}\left(\frac{dV}{ds}\right)$

then, at $s = b$, $\frac{dV}{ds} = \frac{-m'V_{max}{}^6}{0{\cdot}45 \times 0{\cdot}4444V_{max}{}^5 b}$

$$= -\frac{m'V_{max}}{0{\cdot}20b}$$

$$= \frac{-DV_{max}}{(r-1)(Db + E)} \text{ from equation (15).}$$

This condition does not imply continuity of dV/ds at $s = b$ and there is, in fact, a definite suction peak at this point.

Thus $\frac{D}{(r-1)(Db + E)} = \frac{5m'}{b}$.

But $(Db + E)^{1/(r-1)} = \frac{1}{V_{max}}$ from equation (14).

Therefore $D = \frac{5m'(r-1)}{bV_{max}{}^{r-1}}$

and $$E = \frac{1}{V_{\max}^{r-1}}[1 - 5m'(r-1)]$$

$$Ds + E = \frac{1}{V_{\max}^{r-1}}\left[\frac{5m'(r-1)s}{b} + 1 - 5m'(r-1)\right]$$

and the final form of the solution is:

$$V = \frac{V_{\max}}{\left[\frac{5m'(r-1)(s-b)}{b} + 1\right]^{1/(r-1)}}.$$

Expressed in non-dimensional terms this equation reduces to:

$$\frac{V}{V_2} = \frac{k}{\left[5m'(r-1)\left(\frac{s}{b} - 1\right) + 1\right]^{1/(r-1)}} \qquad (16)$$

where $$k = \frac{V_{\max}}{V_2}$$

at the trailing edge $s = S$ and $V = V_2$.

Thus $$1 = \frac{k}{\left[5m'(r-1)\left(\frac{S}{b} - 1\right) + 1\right]^{1/(r-1)}}$$

and $$k = \left[5m'(r-1)\left(\frac{S}{b} - 1\right) + 1\right]^{1/(r-1)} \qquad (17)$$

In this case and in that considered in the next section the velocities considered are those at the edge of the boundary layer, but, as has been explained previously, these velocities correspond to those on the surface in the potential-flow case, so that the velocity distributions obtained should be considered as potential-flow distributions.

The general form for this distribution is shown in Fig. 19 in which a value of 0·01 is taken for b/S amd m' is kept constant at 0·080.

It is of interest to deduce the reduction in velocity from the suction peak to the trailing edge which is possible with this special form of distribution. The following table gives the relationship between k and b for the cases of m constant at 0·080 and 0·070 respectively.

$m' = 0{\cdot}080$

$\frac{b}{S}$	0·001	0·01	0·05	0·10	0·15	0·20
k	2·19	1·77	1·51	1·40	1·34	1·30

$m' = 0{\cdot}070$

$\frac{b}{S}$	0·001	0·01	0·05	0·10	0·15	0·20
k	2·06	1·69	1·46	1·36	1·31	1·27

$k = V_{max}/V_2$ is a measure of the maximum velocity reduction which can be achieved if m' is not to exceed the given constant value.

It does not follow that this form of distribution gives the highest possible lift while adhering to the no-breakaway condition and further mathematical work may provide distributions which do, in fact, give rise to greater lift coefficients. It is likely, however, that with such a distribution it will be necessary to obtain the maximum pressure rise over at least a length of the surface approaching the trailing edge and for this part a curve of the form derived above would be used, modified values for X_1 being required to determine the constants in the equation.

4.3. *Ideal Form for the Velocity Distribution in the Turbulent Layer.*—It has been noted, in the earlier discussion, that losses other than those due to skin friction in the turbulent layer do not become appreciable until after the critical point. Thus, if the critical point can be delayed sufficiently these losses will never occur. The critical point is defined as the point at which $d\theta/ds$ reaches the value $0{\cdot}01$ and it is clear that, if this value is not reached, the critical point will be eliminated. It can also be shown that the maximum pressure rise under these conditions will be obtained if $d\theta/ds$ is maintained at its maximum permissible value throughout.

The form of the distribution for $d\theta/ds = \text{constant} = \phi$ is best derived from the von Kármán momentum equation with an assumed form for the skin-friction coefficient. Hewson has shown (Ref. 3) that the normal equation without the extra term allowing for pressure difference across the boundary layer may be used up to the critical point.

With the usual nomenclature the momentum equation for the boundary layer is:

$$\frac{d\theta}{ds} + (H+2)\frac{\theta}{V_\delta}\frac{dV_\delta}{ds} = \frac{\tau}{\rho V_\delta^2} = \theta T \qquad (18)$$

where V_δ is the local velocity in the main stream at the edge of the boundary layer.

Hewson finds that $\log\left(\frac{R\theta}{R\theta_0}\right) \simeq 0{\cdot}8 \log\left(\frac{\theta}{\theta_0}\right)$. (19)

The values for $\theta_0 T_0$ are given by the Squire and Young Friction Law assuming Tetervin's relation for $\tau/\rho V^2$ (Ref. 3),

i.e., $$\frac{\tau}{\rho V^2} = \left[\frac{\tau}{\rho V^2}\right]_{s=s_0}\left(\frac{\theta_0}{\theta}\right)^{0{\cdot}8t}$$

where the suffix 0 refers to conditions at the beginning of the turbulent layer,

i.e., $$\frac{\tau}{\rho V^2} = \theta_0 T_0 \left(\frac{\theta_0}{\theta}\right)^{0{\cdot}8t} \qquad (20)$$

$\theta_0 T_0$ being given by the Squire and Young Friction Law if

$$\frac{d\theta}{ds} = \text{constant} = \phi .$$

Then $$\theta = \theta_0 + \phi s$$

and equation (18) becomes

$$\phi + (H+2)\frac{(\theta_0 + \phi s)}{V_\delta}\frac{dV_\delta}{ds} = \theta_0 T_0 \left(\frac{\theta_0}{\theta}\right)^{0{\cdot}8t}$$

or $$\frac{\phi\, ds}{\theta_0 + \phi s} + (H+2)\frac{dV_\delta}{V_\delta} = \frac{\theta_0^{(1+0{\cdot}8t)} T_0\, ds}{(\theta_0 + \phi s)^{(1+0{\cdot}8t)}} .$$

For $\theta_0 T_0 = \dfrac{1}{300}$

$(\theta/S)_0$	$(s/S)_0$					
	0	0·10	0·30	0·50	0·70	0·90
0·0002	2·42	2·36	2·22	2·06	1·83	1·46
0·0004	2·06	2·00	1·89	1·76	1·58	1·30
0·0006	1·87	1·83	1·74	1·62	1·46	1·23
0·0008	1·76	1·72	1·63	1·52	1·40	1·18

For $\theta_0 T_0 = \dfrac{1}{350}$

$(\theta/S)_0$	$(s/S)_0$					
	0	0·10	0·30	0·50	0·70	0·90
0·0002	2·52	2·46	2·32	2·14	1·90	1·50
0·0004	2·14	2·08	1·96	1·82	1·62	1·32
0·0006	1·94	1·89	1·79	1·66	1·50	1·24
0·0008	1·82	1·78	1·68	1·57	1·42	1·20

From these tables the importance of the value of θ/S at transition can be appreciated. It is also seen that large pressure rises can be accommodated in the turbulent layer provided the form of the distribution is satisfactory. The general form for this special distribution (Fig. 20) shows that the pressure gradient is large immediately after transition and gradually falls off towards the trailing edge. It is interesting to note that this form is in many ways similar to the ideal form for the laminar layer though pressure gradients in the turbulent case tend to be somewhat larger.

5. *Application of Results.*—5.1. *Applications to Two-dimensional Design.*—It has been made clear from the previous work that, to obtain the most satisfactory pressure distribution for a particular case, all the special features of the case must be considered. The total pressure rise which is a function of the lift is the fundamental item. In addition to this the design Reynolds number and not less important the likely range of Reynolds number must be taken into account.

The results so far have been expressed in terms of velocity and pressure distributions and no direct relations have been established with actual profile shapes. However, it seems apparent that a rational design method must start with the velocity distribution and that the corresponding profile shape and incidence angle must then be derived. A number of mathematical solutions of the inverse potential-flow problem (deriving the aerofoil shape from the velocity distribution) have been devised (*see* Ref. 12). Furthermore the accumulating series of results obtained in electric potential tank measurements should provide a comprehensive fund of data. The potential-flow distribution provides a very sound basis for design although the distribution obtained in the wind tunnel will be modified by boundary-layer effects. It should be appreciated that the boundary layer tends to thicken rapidly where pressure gradients are high and thus tends to reduce these adverse gradients. Designing on the basis of the potential-flow distribution in which pressure gradients are likely to be higher than those actually encountered will thus introduce a certain margin of safety and will render unnecessary long and tedious calculations on boundary-layer developments at several different Reynolds numbers.

5.2. *The Effect of Turbulence.*—The effect of varying degrees of turbulence in the main stream was not investigated in the experimental work. The degree of turbulence actually present was extremely small whereas in compressor practice the flow will be highly turbulent especially at the high-pressure end.

It is widely supposed that increased turbulence merely has the effect of increasing the equivalent Reynolds number. There is some justification for this assumption and it may be considered that the laminar breakaway characteristics will be improved on this account. A more detailed study of turbulence carried out by Martlew (Ref. 13) in this cascade wind tunnel indicates that the assumption of a turbulence factor which increases approximately uniformly with turbulence is an over-simplification. It should be noted that increased turbulence will accelerate the onset of turbulent breakaway thus increasing the importance of that effect as a limiting factor in design considerations.

6. *Conclusions.*—The conclusions of the report are briefly summarised below:

The pattern of flow through diffusing cascades undergoes considerable change with variation of Reynolds number. At low Reynolds number laminar separation occurs causing rapid falling off in the efficiency whilst at higher speeds turbulent separation is a source of increased loss.

The Reynolds numbers at which these effects occur are not even approximately constant but are determined by the form of the potential-flow pressure distribution.

The onset of both laminar and turbulent breakaway can be determined by approximate mathematical boundary-layer theory provided that the transition point is known.

The detailed form of the pressure distribution is important in determining the overall cascade performance especially in relation to Reynolds number. Theoretical methods can be used to derive the most suitable form for the distribution for given conditions of lift and Reynolds number. The most satisfactory general form has, on the suction surface, a well-defined suction peak close to the leading edge with a gradually decreasing pressure gradient towards the trailing edge.

These forms of pressure distribution are sensitive to changes of incidence and the more precise methods of design outlined will result in considerable reduction in the allowed working range of incidence, so that large changes in the pressure distribution due to change of incidence need not be anticipated.

Three-dimensional effects in most low-speed wind tunnels and in compressors are considerable but good correlation with the true two-dimensional case can be obtained by the use of the corrections given in this report.

If a normally small trailing-edge radius is used the circulation may be estimated accurately from the Joukowski condition, unless boundary-layer calculations indicate that separation of either the laminar or turbulent layer is imminent.

The problem of transition is of vital importance in determining cascade performance over the whole speed range and some method of transition prediction is necessary if full use is to be made of theoretical methods in design.

7. *Acknowledgments.*—This investigation was carried out in the Cambridge University Engineering Department.

Acknowledgment is made to the Chief Scientist, Ministry of Supply, for permission to use some test results from research work sponsored by the Ministry.

8. *Nomenclature.*—The nomenclature used in this report is based on that given in Ref. 4. The use of detailed boundary-layer equations leads to duplication of certain of these symbols and some alterations have been made from the list of symbols in Ref. 4. A full list of the notation used is given below :

Symbols

b	Distance of suction peak from leading edge measured along surface of aerofoil
h	Total-head pressure
k	Ratio of velocity at suction peak to outlet velocity
l	Width of stream tube flowing through cascade
m	Thwaites' form parameter for laminar boundary layer
p	Static pressure
s	Distance along surface of aerofoil from leading edge
x	Projected distance along chord line from leading edge
y	Distance measured along plane of cascade
y_p	Blade pitch
C	Chord length
C_D	Drag coefficient
C_L	Lift coefficient
H	Ratio of displacement-thickness to momentum-thickness in boundary layer
L	Lift
S	Distance from leading edge to trailing edge, measured along suction surface of aerofoil
V	Velocity
α	Air angle relative to normal to plane of cascade
δ	Boundary-layer displacement thickness
ε	Air deflection
θ	Boundary-layer momentum thickness
ξ	Contraction ratio
ρ	Density
ν	Kinematic viscosity
τ	Skin-friction coefficient in boundary layer
ϕ	Value of $d\theta/ds$ in boundary layer
ω	Loss of total head
$\bar{\omega}$	Mean loss of total head
Δp	Pressure rise across cascade
Δp_{th}	Theoretical pressure rise

Suffixes

0	Commencement of turbulent boundary layer
1	Inlet to cascade
2	Outlet from cascade
3	Large distance from cascade on outlet side
′	At traverse position
$[\ ]_{\xi=1}$	Values which would occur with true two-dimensional flow

REFERENCES

No.	*Author*	*Title, etc.*
1	H. G. Rhoden	Effects of Reynolds number on the flow of air through a cascade of compressor blades. R. & M. 2919. June, 1952.
2	B. Thwaites	Approximate calculation of the laminar boundary layer. *Aero. Quart.*, Vol. 1. November, 1949.
3	C. T. Hewson	The growth and separation of the turbulent layer. Ph.D. Thesis, Cambridge University. 1949.
4	A. R. Howell	The present basis of axial flow compressor design. Part I, Cascade theory and performance. R. & M. 2095. June, 1942.
5	H. G. Rhoden	The development of a wind tunnel. *Engineering*, Vol. 171, p. 677. June, 1951.
6	J. H. Preston and N. E. Sweeting ..	An improved smoke generator for use in the visualisation of air flow, particularly boundary-layer flow at high Reynolds numbers. R. & M. 2023. October, 1943.
7	W. D. Armstrong	An investigation of secondary flow in cascades of axial flow compressor blades. A.R.C. 15,250. May, 1953.
8	A. D. S. Carter and E. M. Cohen ..	Preliminary investigation into three-dimensional flow through a cascade of aerofoils. R. & M. 2339. February, 1946.
9	A. S. Batson and J. H. Preston ..	The effect of boundary-layer thickness on the normal force distribution of aerofoils, with particular reference to control problems. R. & M. 2008. April, 1942.
10	H. Schlichting	The theory of the boundary layer. Ministry of Supply reprint G.D.C. 10/3011T (TIB Trans. 3472).
11	G. B. Schubauer and H. K. Skramstad	Laminar boundary-layer oscillations and the stability of laminar flow. *Ae. Sci.*, Vol. 14, No. 2, p. 69. February, 1947.
12	R. A. Tyler	The available theoretical analyses of two-dimensional cascade flow. Canadian National Research Council AN—4. 1949.
13	D. L. Martlew	Measurements of the performance of a cascade of compressor blades under various degrees of intensity of turbulence in the incident air stream. A.R.C. 15,249. July, 1952.
14	A. E. Von Doenhoff and N. Tetervin	Determination of general relations for the behaviour of turbulent boundary layers. N.A.C.A. Report 772. 1943.
15	H. M. Garner	The development of turbulent boundary layers. R. & M. 2133. June, 1944.
16	A. Fage and W. G. Raymer	Note on empirical relations for a turbulent boundary layer. R. & M. 2255. March, 1946.

APPENDIX I

Calculation of Mean Values.—Calculation of mean values for total head, etc., from the outlet traverse readings can present a number of anomalies unless the exact method of obtaining a particular mean and the significance of the mean so derived are specified. At the position where the outlet traverses were taken (*i.e.*, a chord length downstream) variations of static pressure across the wake had been virtually damped out and, for the purpose of calculation, this pressure could safely be assumed to be constant over the entire length of the traverse. However, despite the considerable simplification resulting from this, difficulty still existed in computing the correct mean values.

From energy considerations it is clear that the mass flow through the region of high loss (the wake) is proportionally less than that outside the wake and this fact must be allowed for in a computation of the mean energy of the flow. Thus :

Energy transmitted per second through a section of length dy and unit width $= \rho_2' V_2' h_2' \, dy$ where the index $'$ refers to local conditions at the traverse position. Also total flow through a length corresponding to one blade pitch $= \int_y^{y+y_p} \rho_2' V_2' \, dy$.

Mean energy transmitted per unit mass flowing

$$= \frac{\int_y^{y+y_p} \rho_2' V_2' h_2' \, dy}{\int_y^{y+y_p} \rho_2' V_2' \, dy}$$

and mean loss of energy

$$= h_1 - \frac{\int_y^{y+y_p} \rho_2' V_2' h_2' \, dy}{\int_y^{y+y_p} \rho_2' V_2' \, dy}$$

where the suffix 1 refers to conditions at inlet to the cascade.

The resulting loss of energy is a small quantity compared with the energy transmitted and thus a slight error in the calculation of either integral will give a greatly magnified proportionate error in the value of the energy loss. This source of error can be overcome by rearranging the above equation, *i.e.*,

$$\text{mean energy loss} = \frac{\int_y^{y+y_p} \rho_2' V_2' (h_1 - h_2') \, dy}{\int_y^{y+y_p} \rho_2' V_2' \, dy} \qquad \text{(23)}$$

and, since it follows from Bernoulli's equation that the total head remains the same outside the region of viscous effects, the integral in the numerator of the above expression is equal to zero outside the wake. Since the static pressure along the traverse is virtually constant ρ_2' can be assumed to be constant and will cancel out in the above expression. The mean outlet velocity is given by

$$\text{mean} \qquad \bar{V}_2' = V_2 = \frac{1}{y_p} \int_y^{y+y_p} V_2' \, dy \; .$$

Energy per unit mass is equal to total-head pressure expressed in absolute units so that equation (23) gives, in effect a total-head loss. This will be represented by $\bar{\omega}_e$, the suffix e indicating that it has been derived from energy considerations.

The outlet velocity head is thus :

$$\tfrac{1}{2}\rho_2 \bar{V}_2'^2 = h_1 - \bar{w}_e - \rho_2'$$

and a value for the efficiency can now be obtained.

It can be seen at once that the mean outlet velocity head at the traverse position ($= \frac{1}{2}\rho_2 \bar{V}_2'^2$) is not equal to $\frac{1}{2}\rho(\bar{V}_2')^2$ which must give the true value when the wake has eventually been smoothed out into the main stream, since continuity demands that $\bar{V}_2'$ shall remain the same. V_2 and $\bar{V}_2'$ are, in fact, identical but the symbol $\bar{V}_2'$ is used at this stage to emphasise that it is a mean value.

This new value for the outlet velocity head [$\frac{1}{2}\rho_2 \bar{V}_2'^2$] leads to a slightly different value for the total-head loss and the derivation of the corresponding expressions from the momentum equations is described below. The apparent anomaly arising from the differences between these expressions for total-head loss, etc., and those derived previously indicate a limitation of the usefulness of the energy method.

The energy method implies that no further energy is lost after the plane of the outlet traverse and this is, clearly, not the case since further mixing losses must occur. It gives, in fact, the efficiency of the cascade between the two planes considered (the positions for the inlet and outlet traverses). The value of $\bar{\omega}_e$ depends on the rate of decay of the wake and it is likely that at lower speeds the wake will have spread further by the time the outlet traverse plane has been reached. However, provided that the traverse positions are specified, the values for efficiency, etc., given by the above expressions are quite satisfactory for purposes of comparison and have been used where stated in this report.

The expression for total-head loss resulting from considerations of momentum is derived in a similar fashion. The corresponding outlet pressure eventually reaches a slightly different value.

The final expressions are :

$$\bar{\omega}_m = \frac{1}{y_p}\int_y^{y+y_p} \bar{\omega}'\, dy + \frac{1}{4h_1}\left[\int_y^{y+y_p} \frac{\bar{\omega}' + p_2'}{y_p}\, dy\right]^2 \qquad (24)$$

and

$$p_{2m} = p_2' - \frac{1}{2h_1}\left[\int_y^{y+y_p} \frac{\bar{\omega}' + p_2'}{y_p}\, dy\right]^2 \qquad (25)$$

where $\bar{\omega}' = h_1 - \bar{h}_2'$.

The second term in each of these expressions is usually very small and can be neglected so that $\bar{\omega}_m$ is derived from direct integration of the total-head traverse. The value for $\bar{\omega}_m$ is larger than $\bar{\omega}_e$ and the resulting figure for efficiency is smaller.

APPENDIX II

TABLE 1 : *Contraction Coefficients* (ξ)

Cascade camber (deg)	α_1 (deg)	R_n 5·0 × 10⁵			R_n 2·0 × 10⁵			R_n 0·9 × 10⁵		
		α_2	$\alpha_1 - \alpha_2$	ξ	α_2	$\alpha_1 - \alpha_2$	ξ	α^2	$\alpha_1 - \alpha_2$	ξ
40	50	28°35′	21°25′	0·935	28°50′	21°10′	0·924	35°41′	14°19′	0·963
30	50	30°15′	19°45′	0·940	30°04′	19°54′	0·935	30°54′	19°06′	0·942
20	50	30°23′	19°37′	0·936	30°31′	19°29′	0·929	30°37′	19°23′	0·943
40	60	30°00′	30°	0·780	29°49′	30°11′	0·811	30°15′	29°45′	0·796

APPENDIX III

Correction of Pressure Distributions for Stream Contraction

The figure below shows diagrammatically a plan view of the cascade and tunnel.

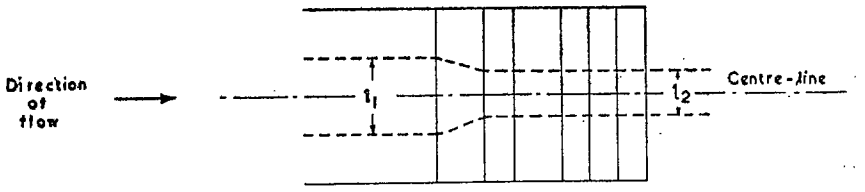

l_1 is the width of a narrow stream tube at the centre of the tunnel (in the plane of traverse) on the inlet side of the cascade and l_2 is the width of the same tube on the outlet side (after contraction). p_δ and V_δ are the local pressure and velocity just outside the boundary layer on the surface of a blade of the cascade. The suffix $[\ ]_{\xi=1}$ refers to conditions which would obtain with two-dimensional flow.

The form of the contraction is defined by the width of the tube at a distance x along the chord line of the blade and this has been taken as : $l_1 - (l_1 - l_2)(x/C)^n$

so that for this position $[V_\delta]_{\xi=1} = \dfrac{l_1 - (l_1 - l^2)}{l_1}\left(\dfrac{x}{C}\right)^n$.

It is also assumed that $\dfrac{l_1}{l_2} = \xi$

and then $\dfrac{[V_\delta]_{\xi=1}}{V_\delta} = 1 - (1 - \xi)\left(\dfrac{x}{C}\right)^n$

and $[V_2]_{\xi=1} = \xi . V_2$.

From Bernoulli the total head outside the boundary layer

$$= h_1 = p_\delta + \tfrac{1}{2}\rho V_\delta^2 = [p_\delta]_{\xi=1} + \tfrac{1}{2}\rho[V_\delta]_{\xi=1}^2 = p_2 + \tfrac{1}{2}\rho V_2^2 = [p_2]_{\xi=1} + \tfrac{1}{2}\rho[V_2]_{\xi=1}^2$$

ρ being taken as constant throughout.

Then $p_\delta - p_2 = \tfrac{1}{2}\rho(V_2^2 - V_\delta^2)$

and $[p_\delta]_{\xi=1} - [p_2]_{\xi=1} = \tfrac{1}{2}\rho([V_2]_{\xi=1}^2 - [V_\delta]_{\xi=1}^2)$.

Subtracting, $([p_\delta]_{\xi=1} - [p_2]_{\xi=1}) - (p_\delta - p_2) = \tfrac{1}{2}\rho(V_\delta^2 - [V_\delta]_{\xi=1}^2 + [V_2]_{\xi=1}^2 - V_2^2)$

and $$\frac{[p_\delta]_{\xi=1} - [p_2]_{\xi=1}}{\tfrac{1}{2}\rho[V_2]_{\xi=1}^2} = \frac{p_\delta - p_2}{\tfrac{1}{2}\rho[V_2]_{\xi=1}^2} + \frac{1}{[V_2]_{\xi=1}^2}(V_\delta^2 - [V_\delta]_{\xi=1}^2 + [V_2]_{\xi=1}^2 - V_2^2).$$

Substituting for $\dfrac{[V_\delta]_{\xi=1}}{V_\delta}$ and $\dfrac{V_2}{[V_2]_{\xi=1}}$,

$$\frac{[p_\delta]_{\xi=1} - [p_2]_{\xi=1}}{\tfrac{1}{2}\rho[V_2]_{\xi=1}^2} = \frac{p_\delta - p_2}{\tfrac{1}{2}\rho V_2^2}\frac{1}{\xi^2} + \frac{V_\delta^2}{[V_2]_{\xi=1}^2}\left\{1 - \left[1 - (1 - \xi)\left(\frac{x}{C}\right)^n\right]^2\right\} + 1 - \frac{1}{\xi^2} .$$

But $$V_\delta^2 = \frac{\tfrac{1}{2}\rho V_2^2 - (p_\delta - p_2)}{\tfrac{1}{2}\rho} .$$

Therefore $\dfrac{[p_\delta]_{\xi=1}-[p_2]_{\xi=1}}{\frac{1}{2}\rho[V_2]_{\xi=1}^2}=\dfrac{1}{\xi^2}\dfrac{(p_\delta-p_2)}{\frac{1}{2}\rho V_2^2}+\left[\dfrac{V_2^2}{[V_2]_{\xi=1}^2}-\dfrac{p_\delta-p_2}{\frac{1}{2}\rho[V_2]_{\xi=1}^2}\right]\left[2(1-\xi)\left(\dfrac{x}{C}\right)^n-(1-\xi)^2\left(\dfrac{x}{C}\right)^{2n}\right]$

$$+1-\frac{1}{\xi^2}=\frac{1}{\xi^2}\frac{(p_\delta-p_2)}{\frac{1}{2}\rho V_2^2}\left[1-(1-\xi)\left(\frac{x}{C}\right)^n\right]^2+\frac{1}{\xi^2}\left[2(1-\xi)\left(\frac{x}{C}\right)^n-(1-\xi)^2\left(\frac{x}{C}\right)^{2n}\right]+1-\frac{1}{\xi^2}$$

$$\frac{[p_\delta]_{\xi=1}-[p_2]_{\xi=1}}{\frac{1}{2}\rho[V_2]_{\xi=1}^2}=1+\frac{1}{\xi^2}\left[1-(1-\xi)\left(\frac{x}{C}\right)^n\right]^2\left[\frac{p_\delta-p_2}{\frac{1}{2}\rho V_2^2}-1\right].$$

It is assumed that the normal pressure on the surface of a blade is equal to the pressure at the corresponding point at the edge of the boundary layer,

i.e., $\quad p_{\text{normal}}=p_\delta=p_n$

where p_{normal} denotes the pressure at the surface.

Then $$\frac{[p_{\text{normal}}]_{\xi=1}-[p_2]_{\xi=1}}{\frac{1}{2}\rho[V_2]_{\xi=1}^2}=1+\frac{1}{\xi^2}\left[1-(1-\xi)\left(\frac{x}{C}\right)^n\right]\left[\frac{p_n-p_2}{\frac{1}{2}\rho V_2^2}-1\right].$$

APPENDIX IV

Reduction of Pressure Rise due to Contraction Effect

Assuming ρ to be constant

$$\frac{[V_2]_{\xi=1}}{[V_1]_{\xi=1}}=\frac{\cos\alpha_1}{\cos\alpha_2}\text{ for two-dimensional flow}$$

$$\frac{V_2}{V_1}=\frac{\cos\alpha_1}{\xi\cos\alpha_2}\text{ with contraction .}$$

Value of Theoretical Pressure Rise.

(i) Using the actual velocities

$$\Delta p_{\text{th}}=\tfrac{1}{2}\rho(V_1^2-V_2^2)$$

$$=\tfrac{1}{2}\rho V_1^2\left(1-\frac{\cos^2\alpha_1}{\cos^2\alpha_2}\frac{1}{\xi^2}\right). \qquad \text{(26)}$$

(ii) Assuming continuity, and

(*a*) basing calculations on V_1

$$\Delta p_{\text{th}}=\tfrac{1}{2}\rho V_1^2\left[1-\left(\frac{\cos\alpha_1}{\cos\alpha_2}\right)^2\right] \qquad \text{(27)}$$

(*b*) basing calculations on V_2

$$\Delta p_{\text{th}}=\tfrac{1}{2}\rho V_2^2\left[\left(\frac{\cos\alpha_2}{\cos\alpha_1}\right)^2-1\right]$$

$$=\tfrac{1}{2}\rho\frac{V_1^2}{\xi^2}\left[1-\left(\frac{\cos\alpha_1}{\cos\alpha_2}\right)^2\right]. \qquad \text{(28)}$$

APPENDIX V

Calculations in the Turbulent Boundary Layer

Available approximate methods and reasons for the choice of Hewson's method.

Though much work is now being carried out in the investigation of the nature of turbulence and the derivation of mathematical theories there is still no exact solution in the case of the turbulent boundary layer.

However, a number of approximate solutions based on the von Kármán momentum equation have been devised, notably those of Doenhoff and Tetervin (Ref. 14) and Garner (Ref. 15). The merits and limitations of both these theories are discussed in detail in a report by Fage and Raymer (Ref. 16). The von Kármán momentum equation, used here in a shortened form,

i.e., $$\frac{d\theta}{ds} + (H + 2)\frac{\theta}{V_\delta}\frac{dV_\delta}{ds} + \frac{\tau}{\rho V_\delta^2} = 0$$

does not give a solution in itself but requires the use of further relations between the variables involved. These further relations are usually obtained from experimental results and take the form of empirical laws relating the local skin-friction coefficient to the local Reynolds number $V_\delta\theta/\nu$ of the turbulent layer and expressing H (the turbulent-layer form parameter) in terms of θ, s, $V_\delta\theta/\nu$, and V_δ.

These extra equations are, at present, purely empirical and are not yet standardised either in form or in the values of the constants used. The von Doenhoff and Tetervin, and Garner methods use different basic equations to supply the extra relations needed. Both these methods are lengthy and tedious though they claim to predict turbulent layer development up to the separation point.

Hewson (Ref. 3) has made a considerable advance by considering the turbulent-layer development in two distinct stages. He has taken account of the pressure gradient across the boundary layer itself, the existence of this pressure gradient being verified by his experiments. Hewson also shows that this pressure gradient inevitably occurs before the separation point is reached but that it is unimportant in the earlier stages of the turbulent layer. The stage at which this pressure gradient across becomes significant is called the Critical Point and is defined as the point at which $d\theta/ds$ reaches the value of $0{\cdot}01$. This definition cannot be regarded as entirely satisfactory but it certainly represents a good approximation to results of Hewson's experiments. It is important to appreciate that these experiments cover many cases in which the turbulent layer is developing against an adverse pressure gradient.

For the purpose of calculation Hewson deals with each stage of the turbulent layer separately. His results make it clear that the difficulties and errors of calculation arise after this critical point. For the first phase he has derived a simple and rapid approximate method using the Squire and Young law for the skin friction (*see* equation 11) and assuming a constant value of H. This approximation gives extremely good results up to the critical point after which the error increases rapidly.

From the critical point up to separation Hewson introduces an extra term into the momentum equation in order to allow for the pressure gradient across the layer.

The extra term is shown to be equal to :

$$\frac{1}{\rho V_\delta^2}\frac{d}{ds}\left(\int_0^\delta (p_n - p_\delta)\, dy_n\right)$$

where y_n is the distance from the surface measured along the normal at a point.

The momentum equation becomes :

$$\frac{d\theta}{ds} + (H + 2)\frac{\theta}{V_\delta}\frac{dV_\delta}{ds} + \frac{\tau}{\rho V_\delta^2} = \frac{1}{\rho V_\delta^2}\frac{d}{ds}\left(\int_0^\delta (p_n - p_\delta)\, dy_n\right).$$

Hewson's solution for the phase from the critical point to separation is obtained by replacing the extra term in the above equation by an approximately equivalent term expressed as a function of the known quantities. A value of 2·65 is assumed for H at separation.

The limitations of the Hewson method are indicated by the large number of approximations involved but it was, nevertheless, considered preferable to the other methods mentioned for the calculations of turbulent-layer development along the blades of the cascade. The reasons for this choice follow from the discussion above and are stated separately below :

(*a*) The location of a critical point which, as is indicated in section 3 of the report, is of importance in itself

(*b*) Ease of calculation up to the critical point

(*c*) The prediction of a separation point is given, by a method derived from experiments carried out in adverse pressure gradients

(*d*) The calculation from the critical point to separation is based on a logical correction for the pressure gradient across the boundary layer itself—a phenomenon whose existence has been verified experimentally.

The full details, work and method are given in the original thesis (Ref. 3).

APPENDIX VI

Values of Rθ at Transition

$R\theta$ is the Reynolds number based on the momentum thickness and the velocity at the edge of the boundary layer,

so that

$$R\theta = \frac{V_\delta \cdot \theta}{\nu}$$

The values of $R\theta$ at transition for a number of cases are shown in the table below :

Cascade camber (deg)	α_1 (deg)	$R\theta$ corresponding to		
		Inlet $R = 5{\cdot}0 \times 10^5$	Inlet $R = 2{\cdot}0 \times 10^5$	Inlet $R = 0{\cdot}9 \times 10^5$
30	60	250	220	193
40	60	280	251	208
40	50	330	261	223

These figures are representative of the whole series of tests and it is seen that there is considerable variation in the value of $R\theta$ at transition. It appears that $R\theta$ at transition increases as the actual inlet Reynolds number is increased and tends to be larger with the less peaky types of pressure distribution.

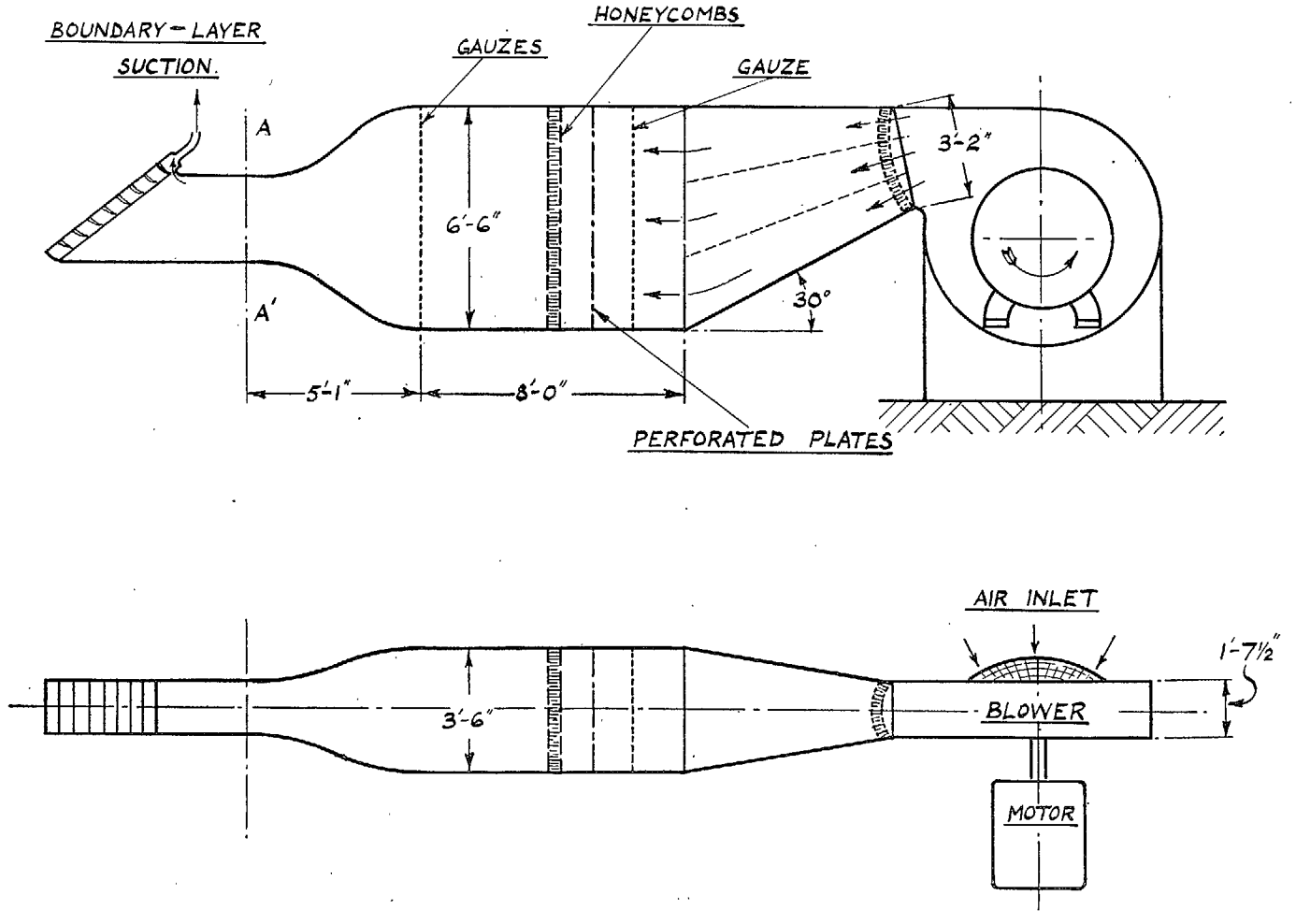

FIG. 1. General arrangement of wind tunnel and cascade.

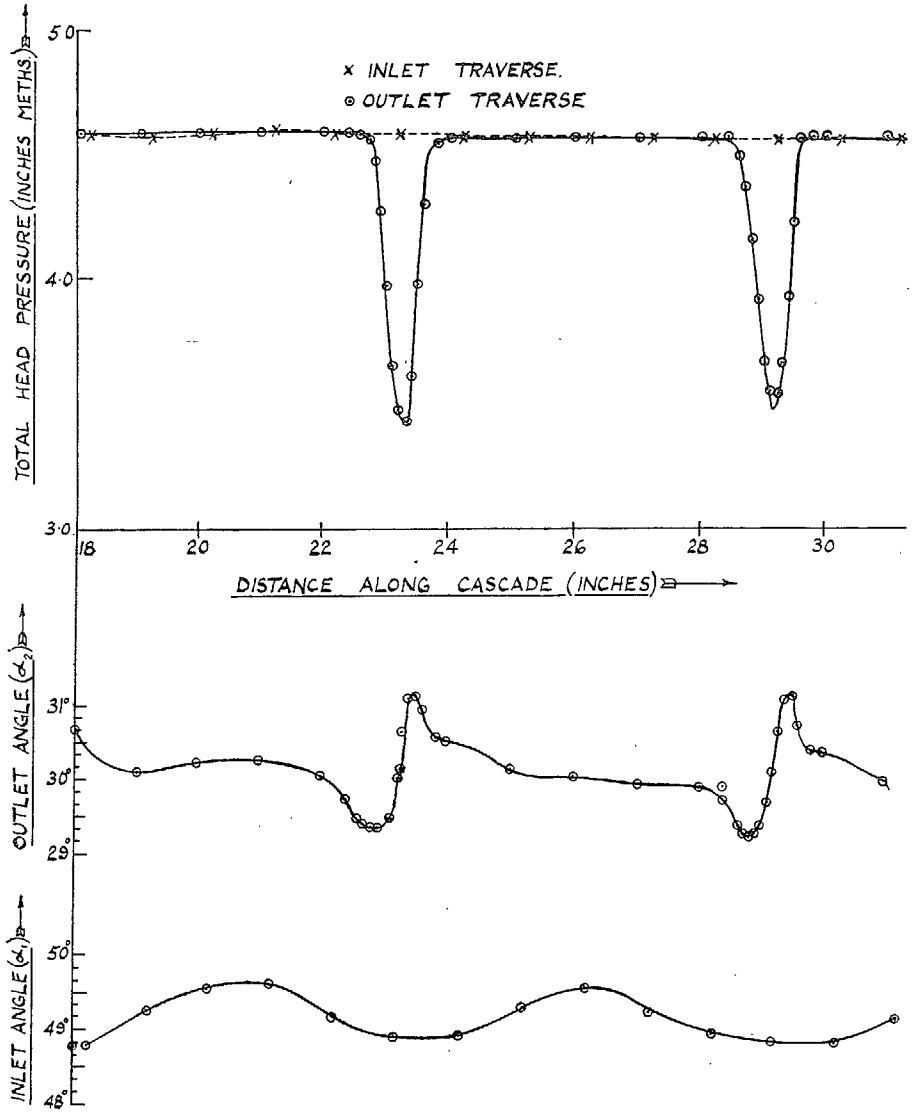

FIG. 2. Typical inlet and outlet traverses. 30-deg camber cascade. $\alpha_1 = 50$ deg. Reynolds number $= 2{\cdot}2 \times 10^5$.

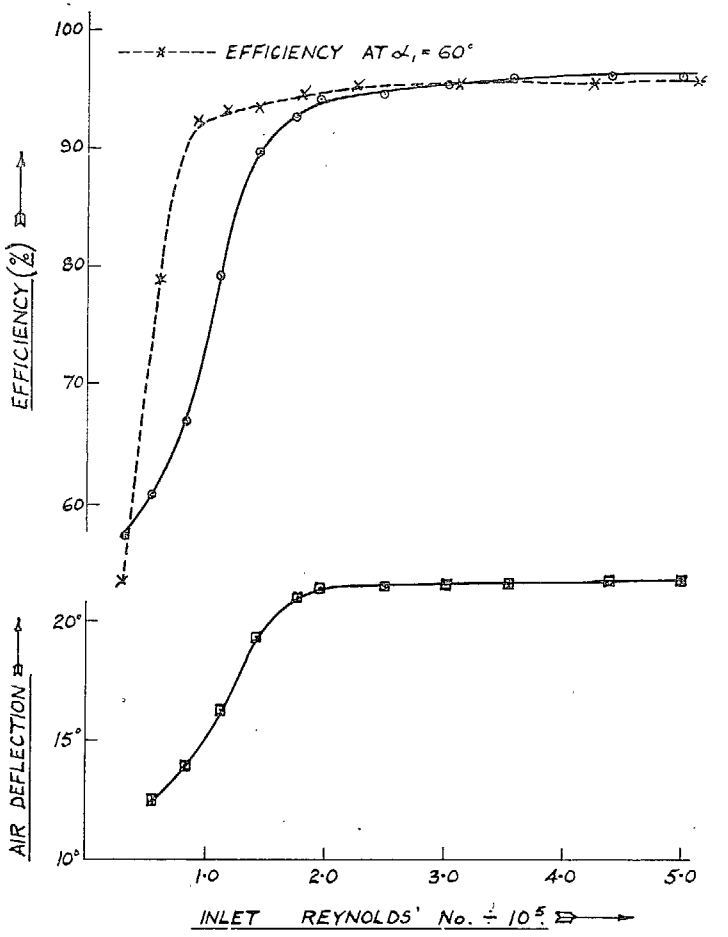

FIG. 3. Curves showing variation of efficiency and air deflection with Reynolds number: taken from results on 40-deg camber cascade at $\alpha_1 = 50$ deg.

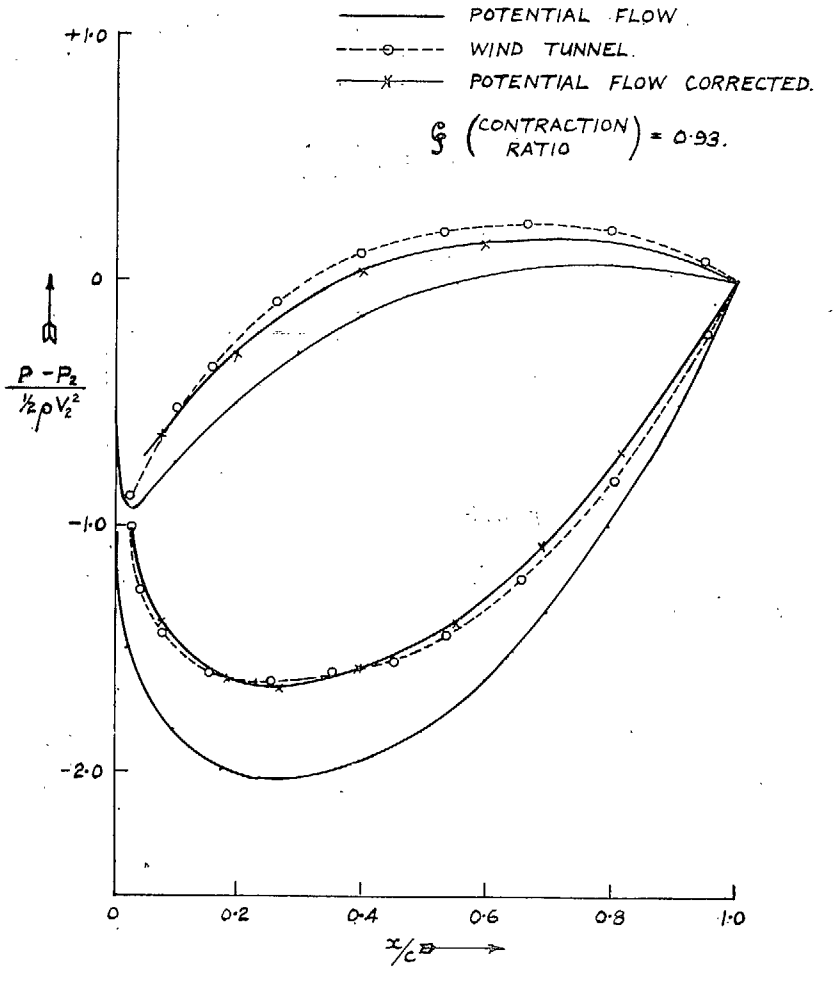

FIG. 4. Comparison of wind-tunnel and potential-flow pressure distributions. 40-deg camber. $\alpha_1 = 50$ deg.

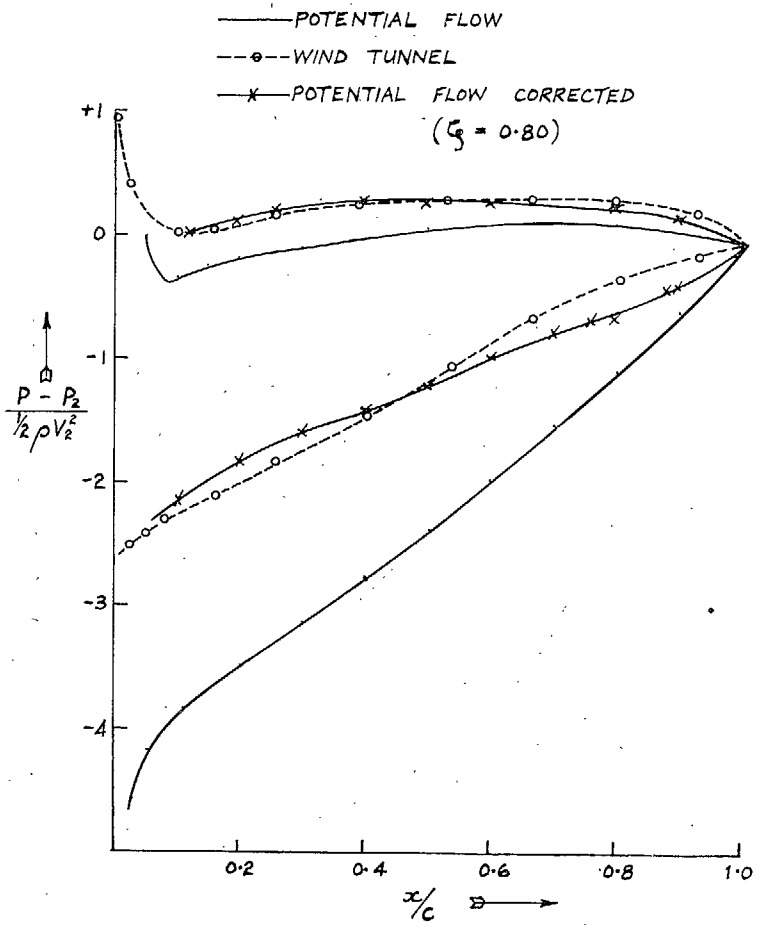

FIG. 5. Comparison of wind-tunnel and potential-flow pressure distributions. 40-deg camber. $\alpha_1 = 60$ deg.

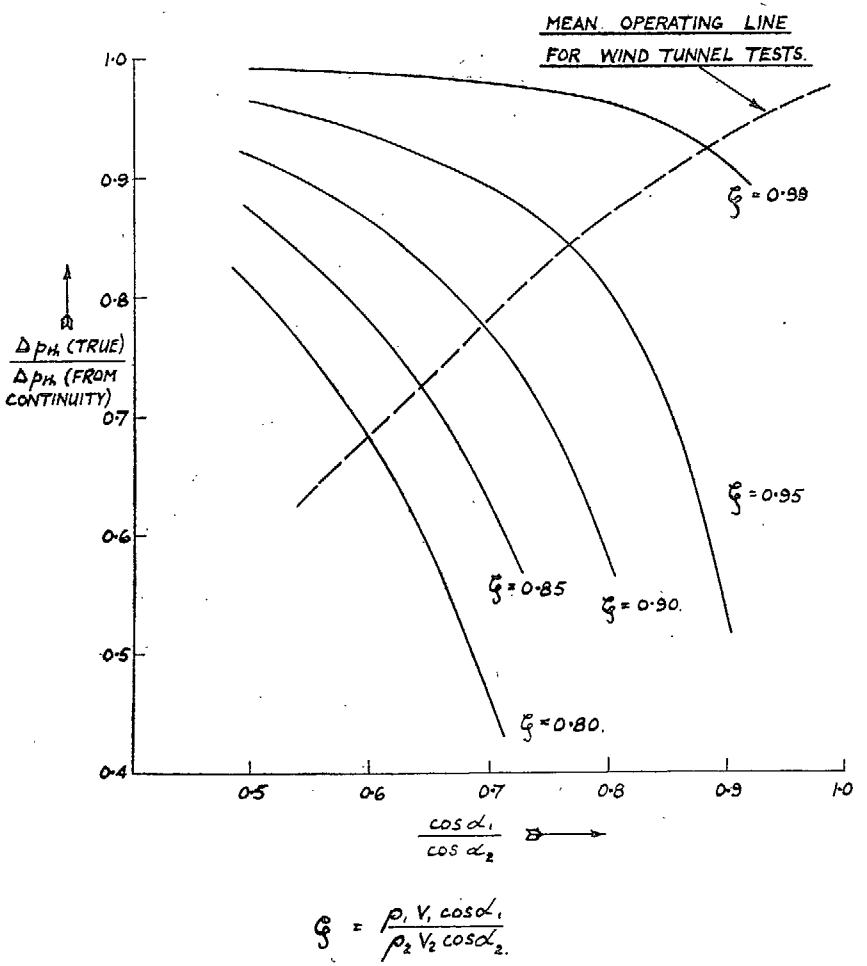

FIG. 6. Three-dimensional effects.
Ratio of true theoretical pressure rise to that calculated assuming continuity and based on inlet conditions ($\frac{1}{2}\rho V_1^2$).

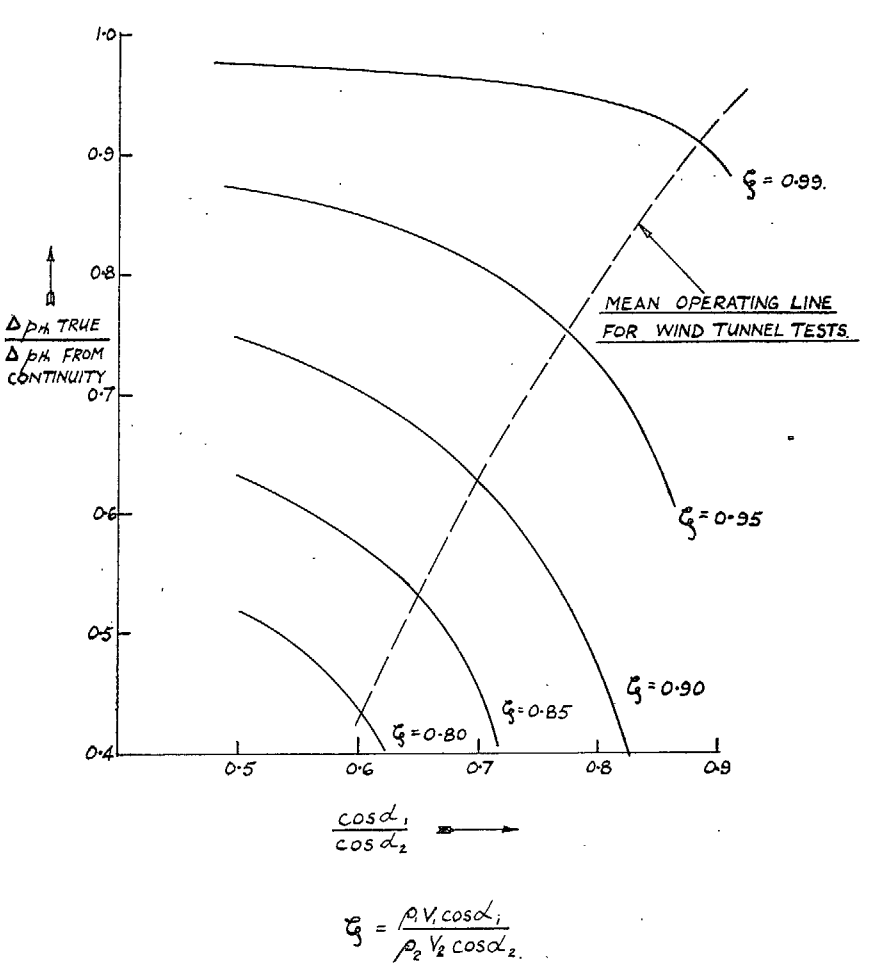

FIG. 7. Three-dimensional effects.
Ratio of the true theoretical pressure rise to that calculated assuming continuity and based on outlet conditions ($\frac{1}{2}\rho V_2^2$).

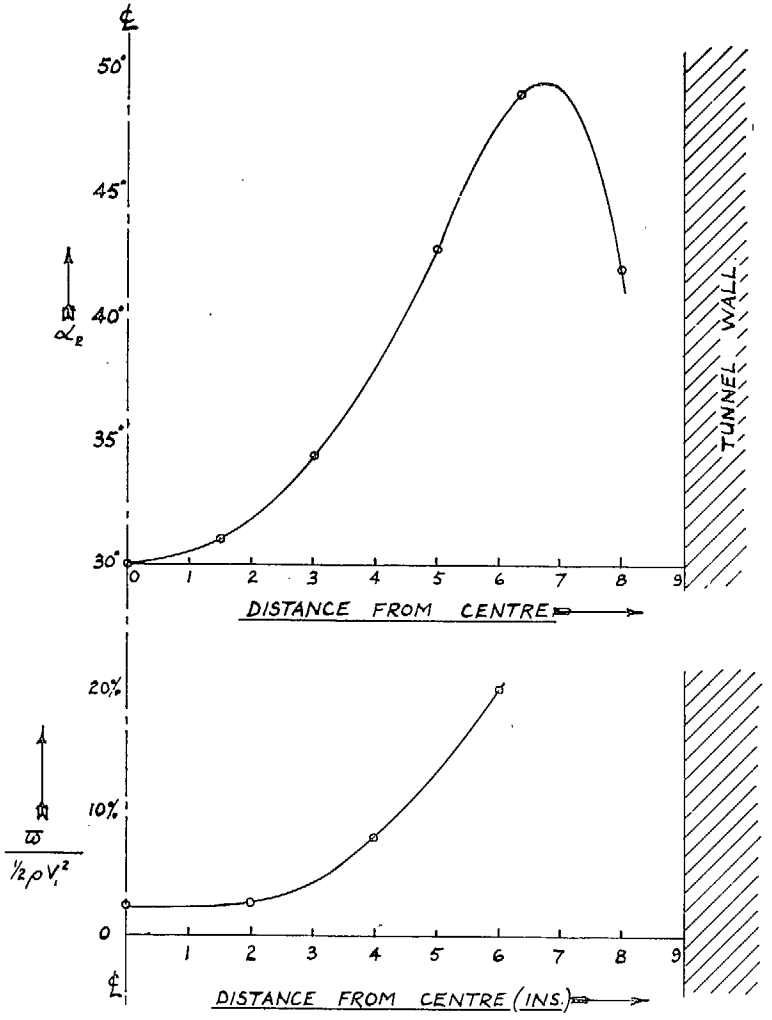

FIG. 8. Three-dimensional effects. Variation of mean α_2 and mean total-head loss across tunnel.

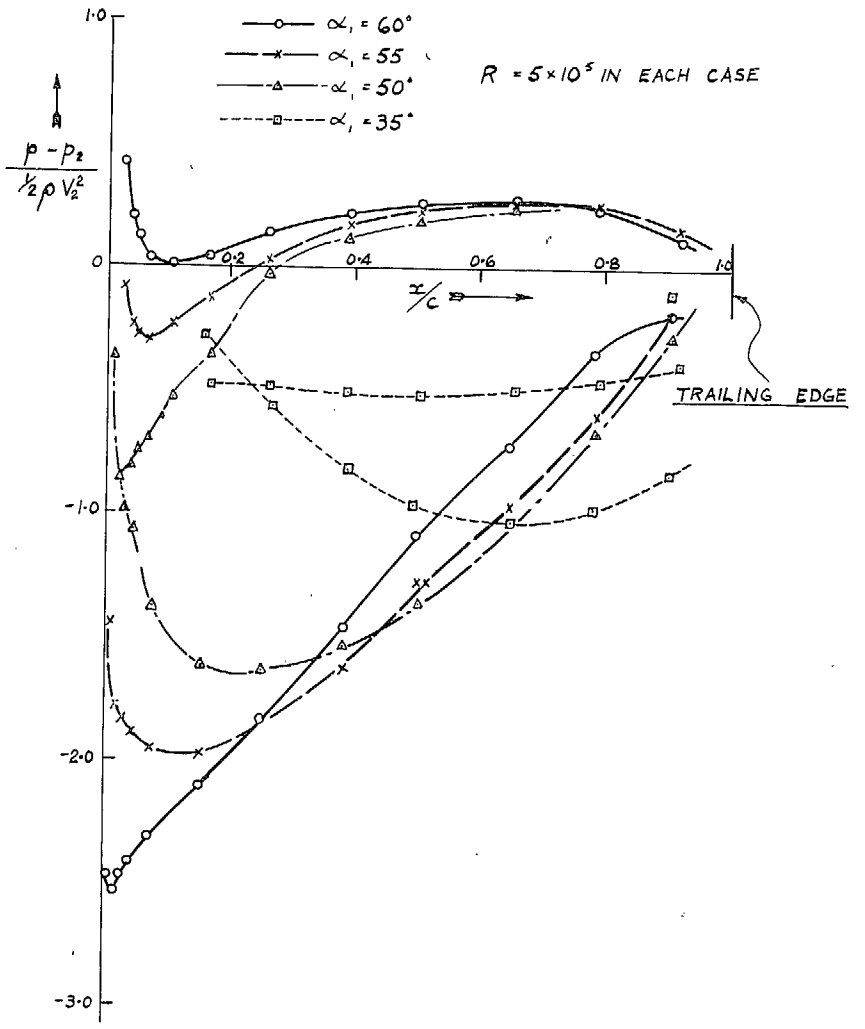

FIG. 9. Effect of incidence angle on pressure distribution. 40-deg camber cascade.

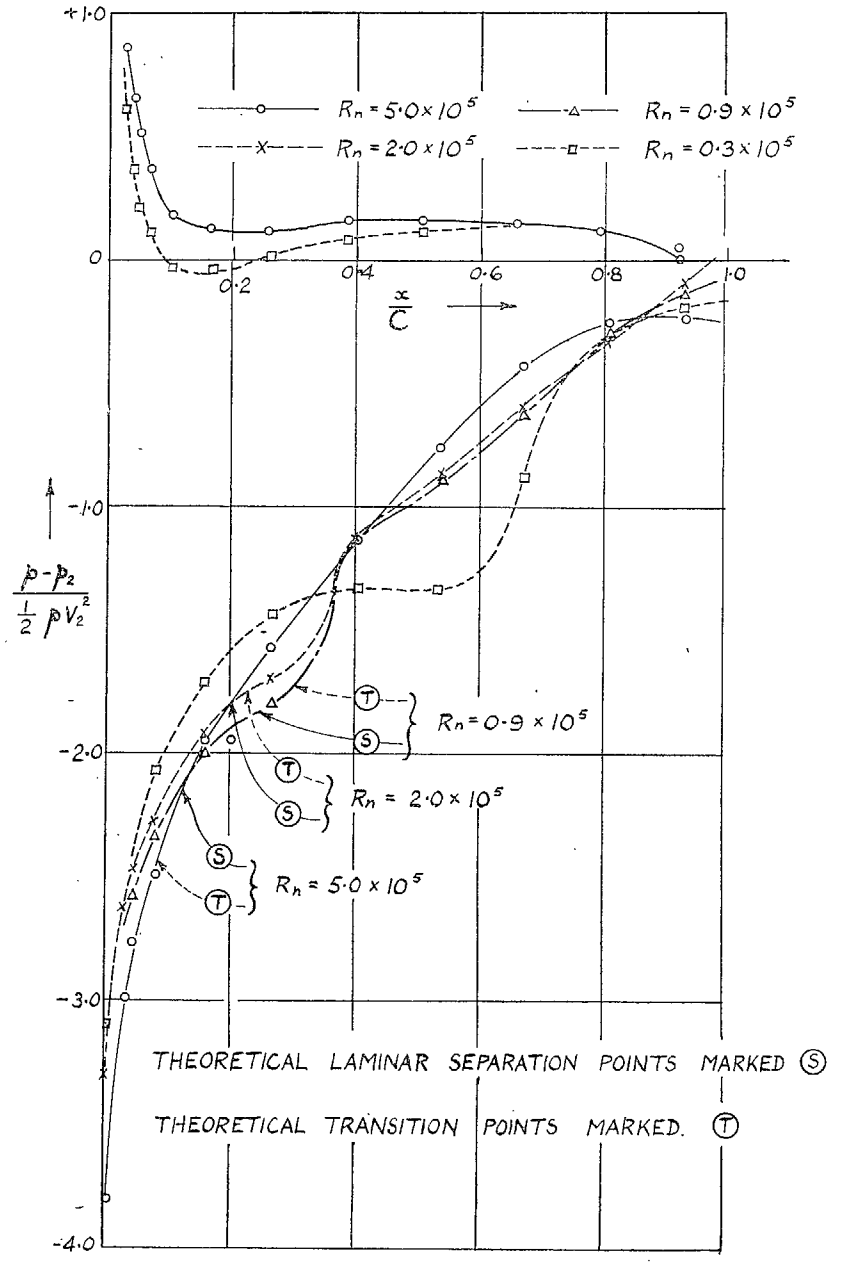

FIG. 10. Effect of Reynolds number on pressure distribution. 30-deg camber cascade. $\alpha_1 = 60$ deg.

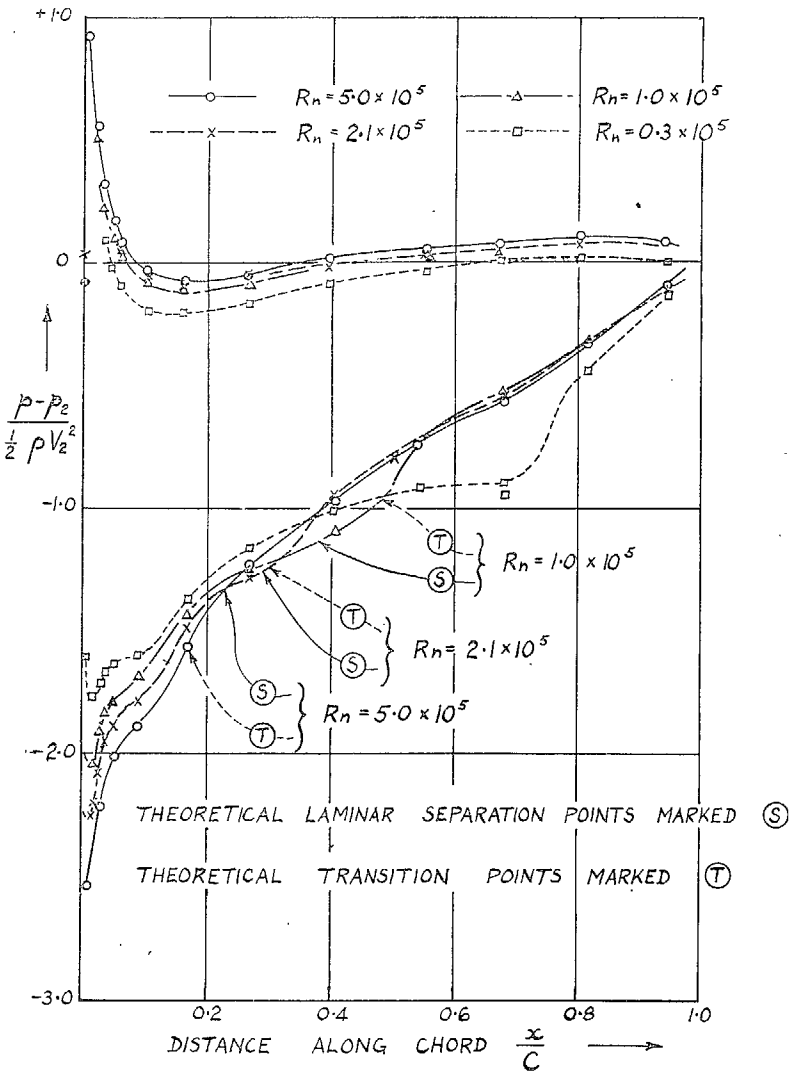

FIG. 11. Effect of Reynolds number on pressure distribution. 20-deg camber cascade. $\alpha_1 = 50$ deg.

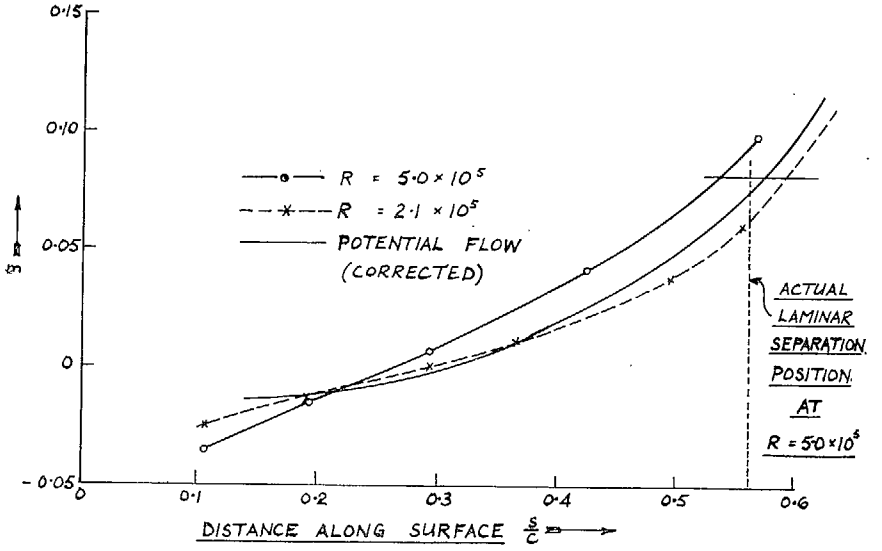

FIG. 12a. 40-deg camber cascade. $\alpha_1 = 50$ deg.

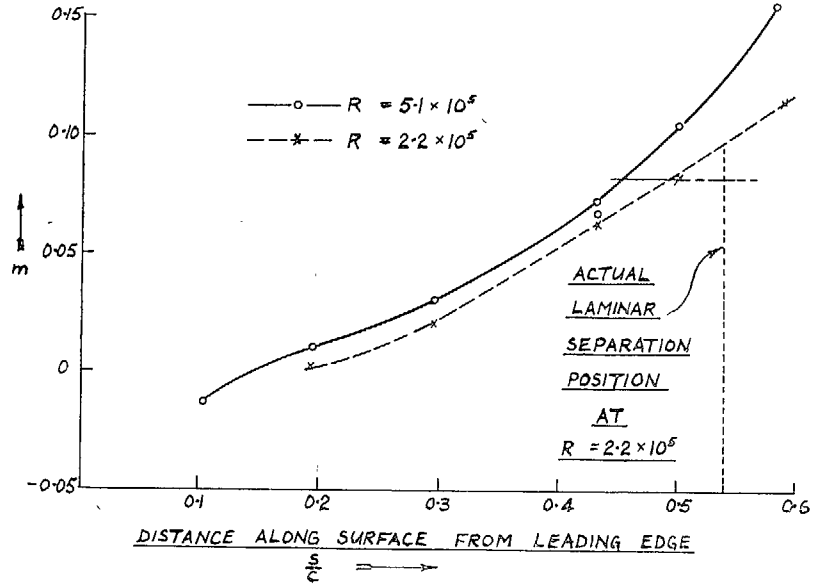

FIG. 12b. 30-deg camber cascade. $\alpha_1 = 50$ deg.

FIGS. 12a and 12b. Laminar separation. Growth of m along suction surface.

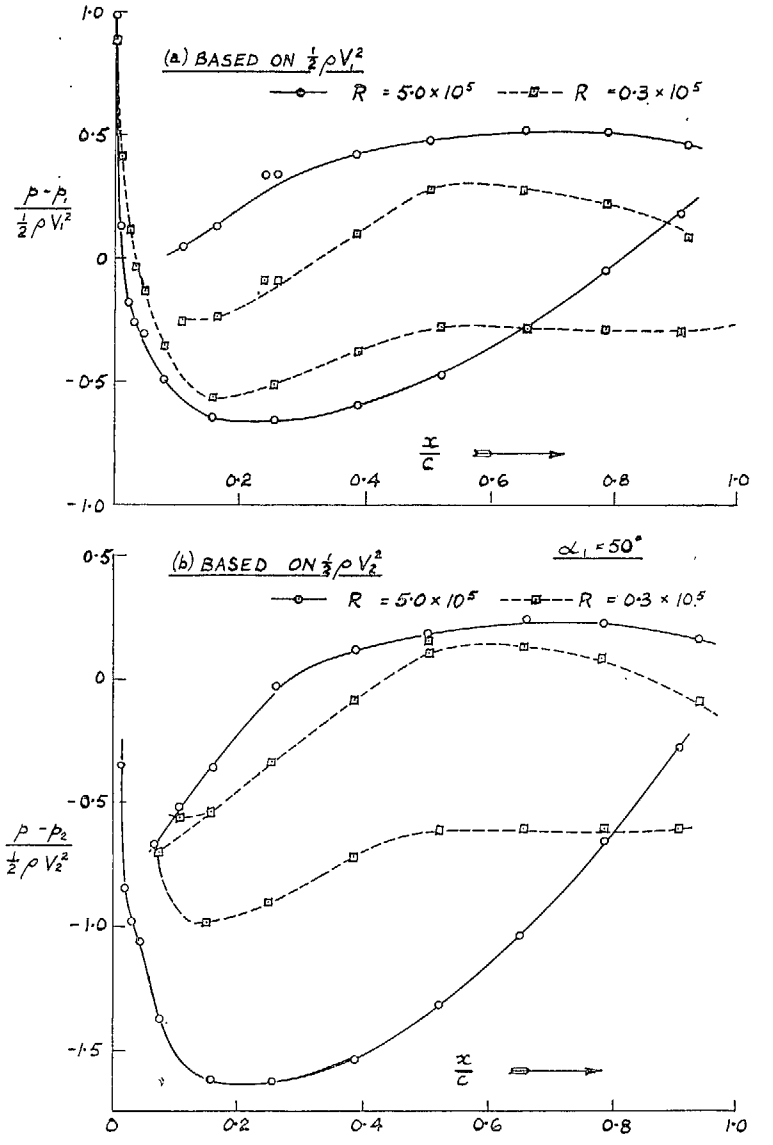

FIG. 13. Comparison of pressure distributions based on $\frac{1}{2}\rho V_1^2$ and on $\frac{1}{2}\rho V_2^2$. 40-deg camber cascade. Inlet angle $\alpha_1 = 50$ deg.

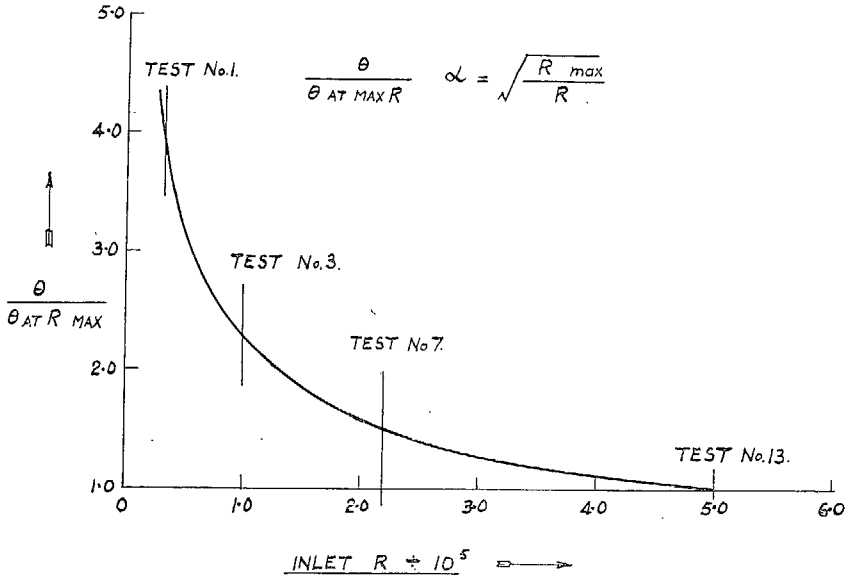

FIG. 14. Relative increase of displacement thickness in laminar layer at reduced Reynolds number.

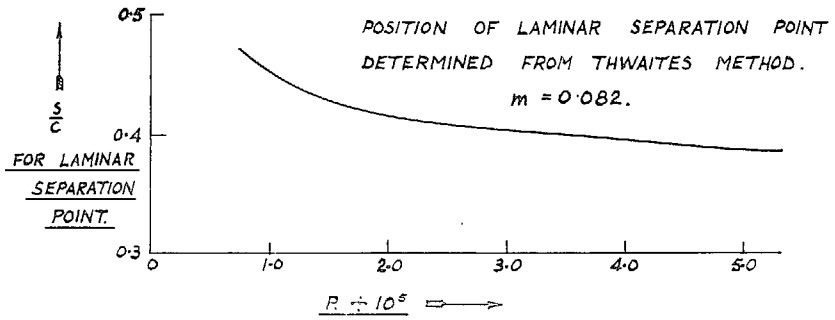

FIG. 15a. 40-deg camber cascade. $\alpha_1 = 50$ deg.

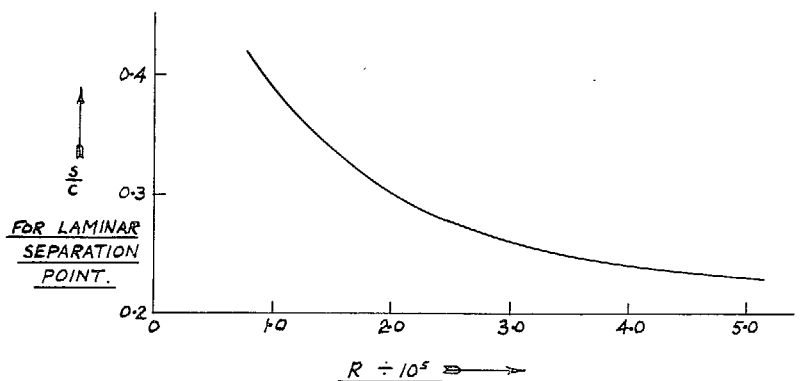

FIG. 15b. 20-deg camber cascade. $\alpha_1 = 50$ deg.

FIGS. 15a and 15b. Movement of laminar separation point with Reynolds number.

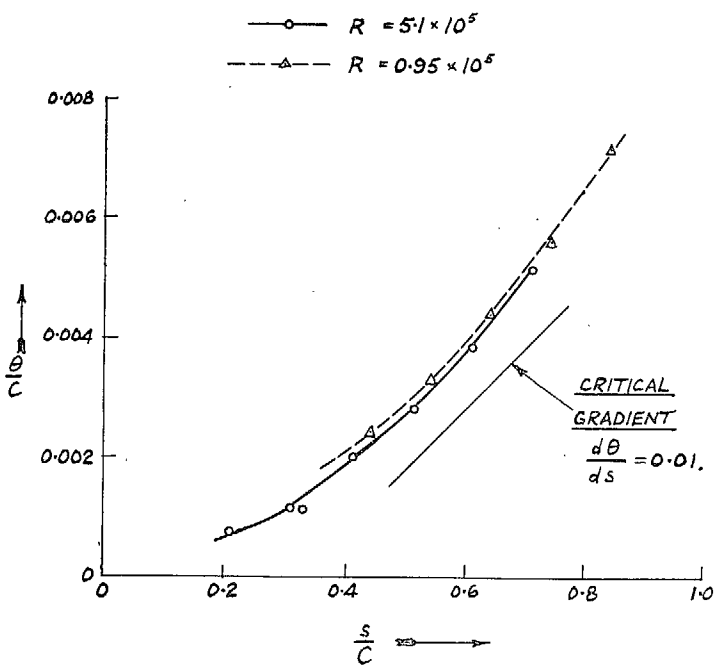

FIG. 16. Growth of momentum thickness in turbulent boundary layer.
30-deg camber cascade. $\alpha_1 = 60$ deg.

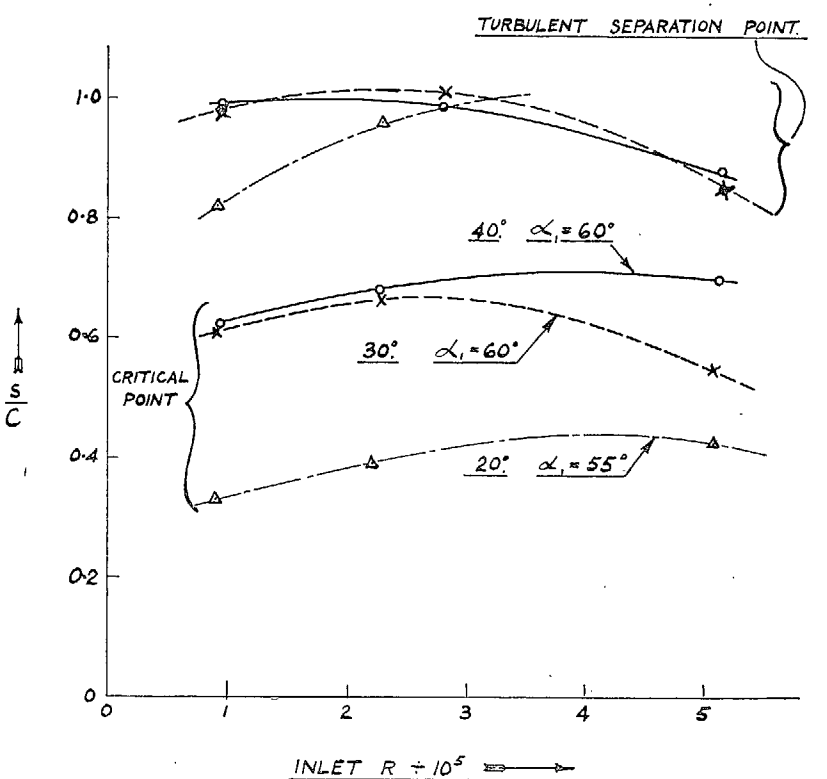

FIG. 17. Turbulent layer characteristics.
Position of critical point and separation point.

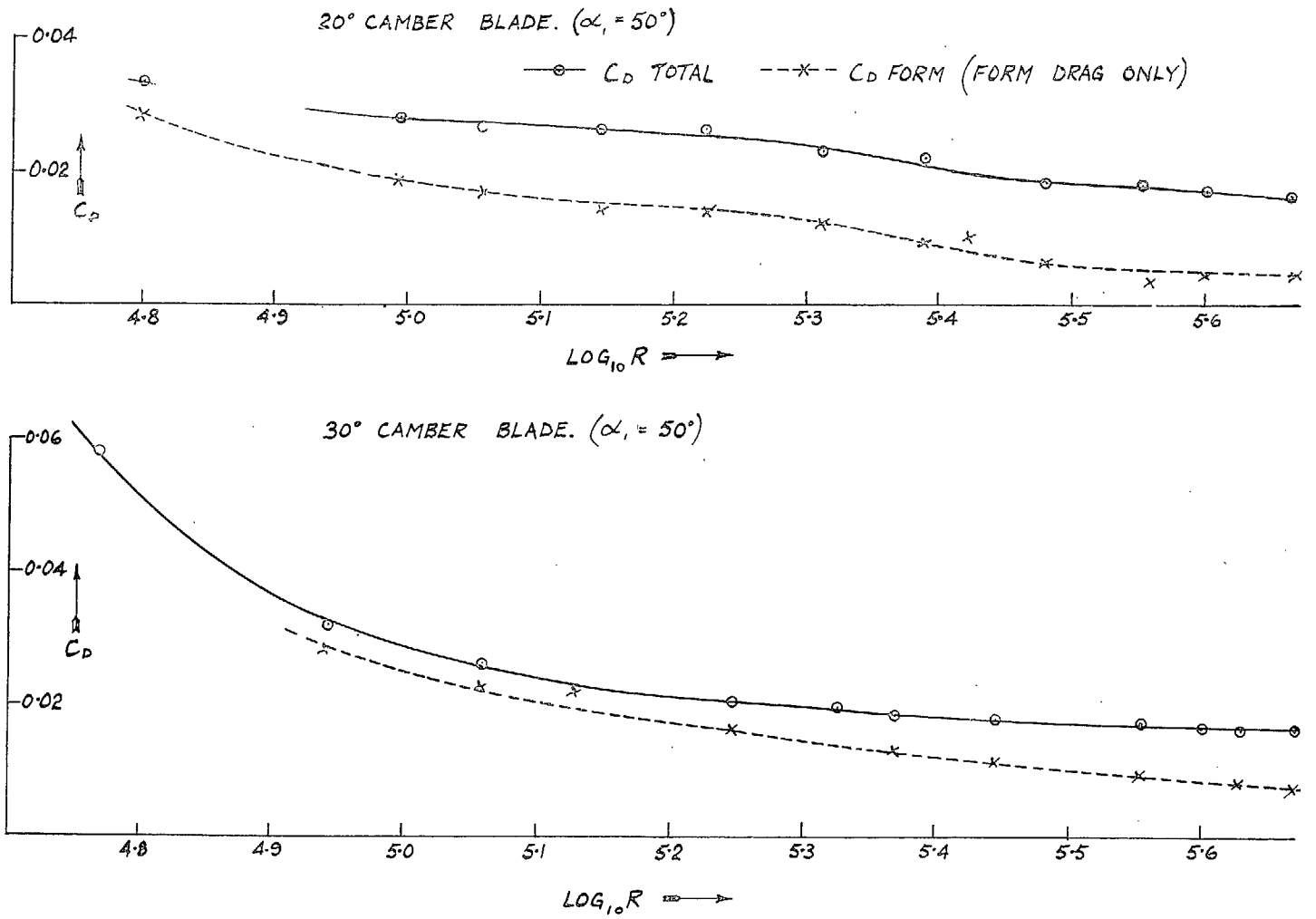

FIG. 18. Corrected drag coefficients of blades in cascade.

J4328 W1.18/9296 K7 9/55 D&Co. 34/263

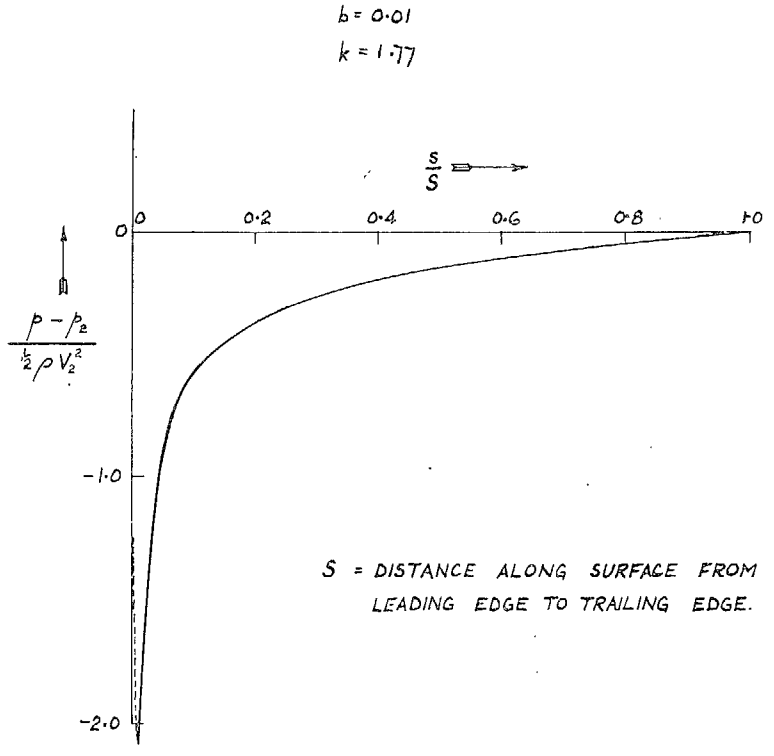

FIG. 19. General form of ' ideal ' pressure distribution for laminar layer.

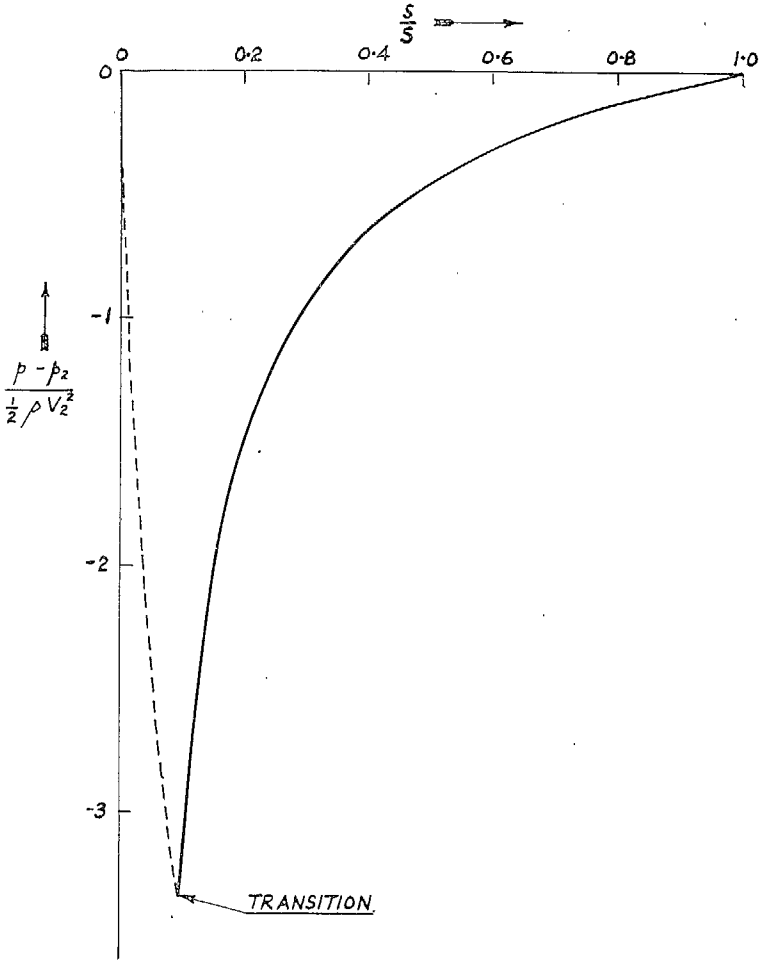

FIG. 20. General form of ideal pressure distribution for the turbulent layer.
$(\theta/S)_0 = 0{\cdot}0004$. $\theta_0 T_0 = 1/350$. $(s/S)_0 = 0{\cdot}1$.

PRINTED IN GREAT BRITAIN

Publications of the Aeronautical Research Council

ANNUAL TECHNICAL REPORTS OF THE AERONAUTICAL RESEARCH COUNCIL (BOUND VOLUMES)

1938 Vol. I. Aerodynamics General, Performance, Airscrews. 50*s*. (51*s*. 2*d*.)
Vol. II. Stability and Control, Flutter, Structures, Seaplanes, Wind Tunnels, Materials. 30*s*. (31*s*. 2*d*.)

1939 Vol. I. Aerodynamics General, Performance, Airscrews, Engines. 50*s*. (51*s*. 2*d*.)
Vol. II. Stability and Control, Flutter and Vibration, Instruments, Structures, Seaplanes, etc. 63*s*. (64*s*. 2*d*.)

1940 Aero and Hydrodynamics, Aerofoils, Airscrews, Engines, Flutter, Icing, Stability and Control, Structures, and a miscellaneous section. 50*s*. (51*s*. 2*d*.)

1941 Aero and Hydrodynamics, Aerofoils, Airscrews, Engines, Flutter, Stability and Control, Structures. 63*s*. (64*s*. 2*d*.)

1942 Vol. I. Aero and Hydrodynamics, Aerofoils, Airscrews, Engines. 75*s*. (76*s*. 3*d*.)
Vol. II. Noise, Parachutes, Stability and Control, Structures, Vibration, Wind Tunnels. 47*s*. 6*d*. (48*s*. 8*d*.)

1943 Vol. I. Aerodynamics, Aerofoils, Airscrews. 80*s*. (81*s*. 4*d*.)
Vol. II. Engines, Flutter, Materials, Parachutes, Performance, Stability and Control, Structures. 90*s*. (91*s*. 6*d*.)

1944 Vol. I. Aero and Hydrodynamics, Aerofoils, Aircraft, Airscrews, Controls. 84*s*. (85*s*. 8*d*.)
Vol. II. Flutter and Vibration, Materials, Miscellaneous, Navigation, Parachutes, Performance, Plates and Panels, Stability, Structures, Test Equipment, Wind Tunnels. 84*s*. (85*s*. 8*d*.)

ANNUAL REPORTS OF THE AERONAUTICAL RESEARCH COUNCIL—

1933–34	1*s*. 6*d*. (1*s*. 8*d*.)	1937	2*s*. (2*s*. 2*d*.)
1934–35	1*s*. 6*d*. (1*s*. 8*d*.)	1938	1*s*. 6*d*. (1*s*. 8*d*.)
April 1, 1935 to Dec. 31, 1936	4*s*. (4*s*. 4*d*.)	1939–48	3*s*. (3*s*. 2*d*.)

INDEX TO ALL REPORTS AND MEMORANDA PUBLISHED IN THE ANNUAL TECHNICAL REPORTS, AND SEPARATELY—

April, 1950 – – – – –	R. & M. No. 2600.	2*s*. 6*d*. (2*s*. 7½*d*.)

AUTHOR INDEX TO ALL REPORTS AND MEMORANDA OF THE AERONAUTICAL RESEARCH COUNCIL—

1909–January, 1954 – – –	R. & M. No. 2570.	15*s*. (15*s*. 4*d*.)

INDEXES TO THE TECHNICAL REPORTS OF THE AERONAUTICAL RESEARCH COUNCIL—

December 1, 1936 — June 30, 1939.	R. & M. No. 1850.	1*s*. 3*d*. (1*s*. 4½*d*.)
July 1, 1939 — June 30, 1945. –	R. & M. No. 1950.	1*s*. (1*s*. 1½*d*.)
July 1, 1945 — June 30, 1946. –	R. & M. No. 2050.	1*s*. (1*s*. 1½*d*.)
July 1, 1946 — December 31, 1946.	R. & M. No. 2150.	1*s*. 3*d*. (1*s*. 4½*d*.)
January 1, 1947 — June 30, 1947. –	R. & M. No. 2250.	1*s*. 3*d*. (1*s*. 4½*d*.)

PUBLISHED REPORTS AND MEMORANDA OF THE AERONAUTICAL RESEARCH COUNCIL—

Between Nos. 2251–2349. – –	R. & M. No. 2350.	1*s*. 9*d*. (1*s*. 10½*d*.)
Between Nos. 2351–2449. – –	R. & M. No. 2450.	2*s*. (2*s*. 1½*d*.)
Between Nos. 2451–2549. – –	R. & M. No. 2550.	2*s*. 6*d*. (2*s*. 7½*d*.)
Between Nos. 2551–2649. – –	R. & M. No. 2650.	2*s*. 6*d*. (2*s*. 7½*d*.)

Prices in brackets include postage

HER MAJESTY'S STATIONERY OFFICE

York House, Kingsway, London W.C.2; 423 Oxford Street, London W.1 (Post Orders: P.O. Box 569, London S.E.1); 13a Castle Street, Edinburgh 2; 39 King Street, Manchester 2; 2 Edmund Street, Birmingham 3; 109 St. Mary Street, Cardiff; Tower Lane, Bristol 1; 80 Chichester Street, Belfast, *or through any bookseller*

S.O. Code No. 23-2920